

Initial Evaluation of Mechanical Stress Distributions in Spent CANDU Fuel Bundles

NWMO TR-2010-11

June 2010

Timothy Lampman and Adrian Popescu

AMEC NSS Limited

nwmo

NUCLEAR WASTE
MANAGEMENT
ORGANIZATION

SOCIÉTÉ DE GESTION
DES DÉCHETS
NUCLÉAIRES



Nuclear Waste Management Organization
22 St. Clair Avenue East, 6th Floor
Toronto, Ontario
M4T 2S3
Canada

Tel: 416-934-9814
Web: www.nwmo.ca

Initial Evaluation of Mechanical Stress Distributions in Spent CANDU Fuel Bundles

NWMO TR-2010-11

June 2010

Timothy Lampman and Adrian Popescu
AMEC NSS Limited

Disclaimer:

This report does not necessarily reflect the views or position of the Nuclear Waste Management Organization, its directors, officers, employees and agents (the "NWMO") and unless otherwise specifically stated, is made available to the public by the NWMO for information only. The contents of this report reflect the views of the author(s) who are solely responsible for the text and its conclusions as well as the accuracy of any data used in its creation. The NWMO does not make any warranty, express or implied, or assume any legal liability or responsibility for the accuracy, completeness, or usefulness of any information disclosed, or represent that the use of any information would not infringe privately owned rights. Any reference to a specific commercial product, process or service by trade name, trademark, manufacturer, or otherwise, does not constitute or imply its endorsement, recommendation, or preference by NWMO.

ABSTRACT

Title: Initial Evaluation of Mechanical Stress Distributions in Spent CANDU Fuel Bundles
Report No.: NWMO TR-2010-11
Author(s): Timothy Lampman and Adrian Popescu
Company: AMEC NSS Limited
Date: June 2010

Abstract

This report describes an initial analysis of the mechanical stress distributions in irradiated 28-element fuel bundles at the start of interim dry storage. The finite element CANDU fuel bundle models previously developed using unirradiated material properties have been updated to include irradiation effects, such as material properties to account for fast-neutron irradiation and consideration of changes to the original bundle geometry following irradiation. Calculations of the stress distribution were performed for different post-discharge bundle geometries modelled under initial dry storage conditions. From the stress distributions within the CANDU fuel bundles, stress intensity factors for the weld notch of the endplate-to-endcap welds were performed for future comparison with experimentally-determined critical stress intensity factors required for delayed hydride cracking.

There are uncertainties related to modelling irradiated fuel elements and where these are considered potentially significant, a conservative approach was used to bound the expected stress levels and intensity factors. The analysis indicates that the endplate-to-endcap welds act as stress concentrators and at the endplate-to-endcap welds, the calculated stress intensity factors did not exceed approximately $3 \text{ MPa m}^{1/2}$.

TABLE OF CONTENTS

	<u>Page</u>
ABSTRACT	v
1. INTRODUCTION.....	1
2. DESCRIPTION OF SPENT CANDU FUEL BUNDLE MODEL.....	3
2.1 Material Properties of Irradiated Zircaloy-4 and UO₂.....	3
2.1.1 Zircaloy-4 Material Properties.....	3
2.1.2 Uranium Dioxide Material Properties	4
2.2 Spent Fuel Bundle Geometries	4
2.3 Fuel Element Models	7
2.3.1 Mechanical Loads for Comparison of Fuel Element Models	7
2.3.2 Comparison of Fuel Element Models.....	8
3. ANALYSIS OF SPENT CANDU FUEL BUNDLES DURING DRY STORAGE ...	11
3.1 Typical Fuel Bundle Geometry Stress Distributions	11
3.1.1 Spent Fuel Bundle Geometries	12
3.1.2 Nominal Fuel Bundle in a Module Tube.....	16
3.1.3 Spent Fuel Bundle in a Module Tube	22
3.2 Crept Channel Fuel Bundle Geometry Stress Distributions	25
3.3 Atypical Fuel Bundle Geometries	31
4. SUMMARY AND DISCUSSION OF FINDINGS	32
5. ACKNOWLEDGEMENTS	34
REFERENCES	35

LIST OF TABLES

	<u>Page</u>
Table 1: Zircaloy-4 Elastic Modulus Values.....	4
Table 2: Comparison of Fuel Element Models under Bending Loads.....	10
Table 3: Post-Discharge Assembly Weld Maximum Stress Intensity Factors for a Crack Depth of 0.5 mm.....	16
Table 4: Calculated Assembly Weld Maximum Stress Intensity Factors for a Nominal 28-Element Bundle in a Module Tube.....	20
Table 5: Calculated Assembly Weld Maximum Stress Intensity Factors for an Average-Burnup 28-Element Bundle in a Module Tube.....	23
Table 6: Calculated Assembly Weld Maximum Stress Intensity Factors for a Crept-Channel Geometry Bundle in a Module Tube.....	26

LIST OF FIGURES

	<u>Page</u>
Figure 1: Ontario Power Generation Dry Storage Container (Birch <i>et al.</i> , 2008).	2
Figure 2: ANSYS Finite Element Model of a Bowed Fuel Element.....	5
Figure 3: Initial Geometry of High-Burnup Bundle 28A.....	6
Figure 4: Initial Geometry of Average-Burnup Bundle 28B.....	6
Figure 5: Fuel Element Model Comparison Loads and Boundary Conditions.....	9
Figure 6: 28-Element Outer Ring Element Submodel Geometry.....	10
Figure 7: Mid-Bundle Cross Section of Post-Discharge 28-Element Bundle Geometry.....	13
Figure 8: Total Displacement of the Fuel Elements at the Bundle Mid-Plane.....	14
Figure 9: Endplate von Mises Stress Distribution Due to Post-Discharge Geometry.....	15
Figure 10: Endplate Axial Stress Distribution Due to Post-Discharge Geometry.....	17
Figure 11: Cross Section of a 28-Element Fuel Bundle in a Module Tube.....	18
Figure 12: Nodal Constraints Applied to Model to Simulate Contact with Module Tube.....	19
Figure 13: Total Displacement of the Fuel Elements in the Bundle Mid-Plane.....	20
Figure 14: Stress Distribution in the Endplate of Nominal Bundle in a Module Tube.....	21
Figure 15: Nodal Constraints to Model the Module Tube for an Average-Burnup Bundle Geometry.....	23
Figure 16: Stress Distributions in the Endplate for Average-Burnup Bundle in Module Tube.....	24
Figure 17: Model Setup for Simulating Crept-Channel Bundle Geometry in a Module Tube.....	26
Figure 18: Nodal Constraints Applied to Crept-Channel Bundle Geometry Model.....	27
Figure 19: Displacement of the Fuel Bundle Viewed Along Bundle Axis.....	28
Figure 20: Displacement of the Fuel Bundle Elements From Side View (units in mm).....	29
Figure 21: Endplate Stress Distribution for Crept-Channel Bundle Geometry.....	30

1. INTRODUCTION

This technical report describes the results of an analysis to better understand the stress levels and stress intensity factors at sharp notches in the endplate-to-endcap welds for spent CANDU fuel bundles during interim storage in a Dry Storage Container (DSC). This work is part of the Used Fuel Integrity (UFI) program at the Nuclear Waste Management Organization (NWMO), which was initiated to provide assurance that spent CANDU fuel which may be stored in a dry environment for up to 100 years can be safely and efficiently handled during post-storage operations. Another project managed by Kinectrics within the UFI program is currently determining the stress levels in fuel bundle materials that are required to initiate Delayed Hydride Cracking (DHC). The calculated stress intensity factors (K_I) from this analysis will be combined with the critical stress intensity factor required for DHC initiation at a crack tip (K_{IH}) to evaluate whether this cracking mechanism may occur in used fuel during the dry storage period.

Past investigations into the condition of CANDU fuel during dry storage have provided confidence that bundles do not significantly degrade and their integrity is maintained under normal storage conditions (Lovasic and Villagran, 2004; Lampman *et al.*, 2005). However, more recent work in the UFI program indicated that fuel bundles stored horizontally in dry storage might be susceptible to delayed hydride cracking, particularly in the endcap-to-endplate welds (commonly termed the *assembly welds*). As a result, a strategy to investigate this degradation mechanism was developed in order to assess whether DHC could occur during dry storage (Lampman *et al.*, 2005).

Delayed hydride cracking is a hydrogen-assisted cracking mechanism which is essentially driven by hydride formation and fracture in high stress fields. There are two basic conditions that must be satisfied for DHC to occur: the concentration of hydrogen in the cracking region must exceed the hydrogen solubility, and there must be sufficient stress to fracture the hydrides that form as hydrogen precipitates out of solution. The concentration of hydrogen isotopes in spent fuel is greater than the solubility for expected dry-storage temperatures. Therefore, to understand whether DHC can occur, the stress levels in the bundles need to be understood and compared against stress levels required to fracture the hydrides. The finite element CANDU fuel bundle models developed (Lampman *et al.*, 2009; Popescu and Lampman, 2009) are tools to evaluate the stress levels present in used fuel during dry storage.

In theory, DHC could occur anywhere in the Zircaloy-4 structural material of the fuel bundles under the right conditions. However, regions of stress concentration, pre-existing flaws or cracks in the material for example, are the most likely place where DHC can occur. Analysis of the bundle geometry prior to dry storage suggests that the most likely place for DHC to occur is at the assembly welds. A typical result of the welding process for assembly welds is a notch with a tip radius on the order of several microns. Finite element submodels were developed to more accurately model the assembly weld regions of a bundle. A weld crack¹ was included in the submodels with a special mesh to allow for the calculation of stress intensity factors.

A description of finite element CANDU fuel bundle models has been documented elsewhere (Lampman *et al.*, 2009; Popescu and Lampman, 2009). The past documentation provides a description of the fuel bundle geometries and the finite element approach used to model the

¹ The weld notch is very sharp and has been conservatively assumed to be a crack in the finite element model. This terminology is used throughout the remainder of this report.

bundles. Several validation tests and experiments were performed to validate the models. A sensitivity study of the model was performed to determine the parameters that have the greatest effect on the bundle response and determine best-fit parameters to be used in the finite element models. Comparison of the unirradiated fuel bundle models with experimental data shows good agreement for axial and bending loads.

This document presents the results of finite element simulations of used 28-element fuel bundles in dry storage performed with the ANSYS 11.0 finite element package. During the interim dry storage period, the fuel bundles will be stored in modules stacked within a DSC, as shown in Figure 1. The fuel bundles are loaded into horizontal module tubes with an inner diameter of 105 mm. The bundles are supported by the module tube and no axial forces are applied on them. The temperature of the fuel bundles varies with time, both seasonally and due to decreasing decay heat of the bundles, but the maximum expected temperature at the start of dry storage is approximately 130°C. DHC initiation is expected to be relatively insensitive to temperature, but the crack propagation velocity increases with temperature. If DHC is present in dry storage, crack growth is expected to initiate at the start of storage. Therefore, the initial dry storage temperature of 130°C was used for this analysis.

Different fuel bundle geometries were evaluated to estimate the range of stress that could be present in the fuel bundle endplates during dry storage. Calculation of the stress intensity factors at the assembly weld cracks was also performed using the assembly weld submodels for future comparison against critical stress intensity factors required for DHC.

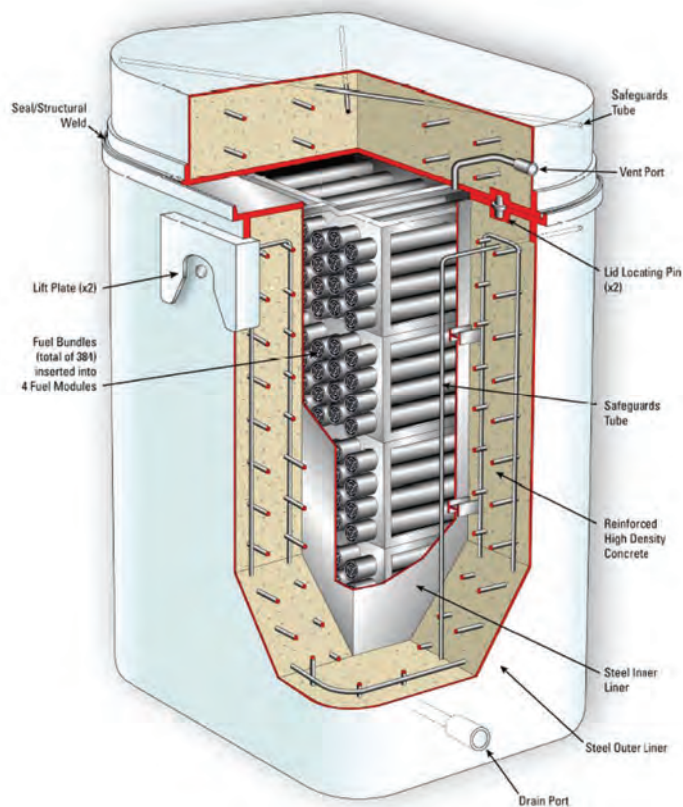


Figure 1: Ontario Power Generation Dry Storage Container (Birch *et al.*, 2008).

2. DESCRIPTION OF SPENT CANDU FUEL BUNDLE MODEL

The finite element models developed to evaluate the mechanical stress distributions and associated stress intensity factors for sharp flaws at the assembly welds of unirradiated 28- and 37-element CANDU fuel bundles have been described previously (Lampman *et al.*, 2009; Popescu and Lampman, 2009). In summary, finite element models of the entire bundle structure (termed the *full bundle model*) and more finely meshed models of the assembly welds (termed the *weld submodel*) were created using ANSYS Parametric Design Language (APDL) scripts. The geometry and material properties are defined as parameters in the APDL scripts. In addition, each major component of the fuel bundle is modelled separately. The entire model structure is created by combining the separate models for each component. This approach provides flexibility in defining models that are created for specific analysis purposes.

For the work discussed in this report, the key aspects of the fuel bundle models that are varied are:

1. material properties to account for the effects of irradiation and temperature;
2. fuel element bowing in the plane perpendicular to the bundle axis to account for post-reactor-discharge bundle geometry; and
3. fuel element models to account for the effect of fuel pellet interactions with the fuel element sheath and adjacent pellets.

These aspects as they relate to the spent CANDU fuel bundle models are discussed in the following subsections.

2.1 Material Properties of Irradiated Zircaloy-4 and UO₂

The material properties of Zircaloy-4 and UO₂ for the unirradiated fuel bundle models (Lampman *et al.*, 2009) were taken from MATPRO (MATPRO, 1990). The elastic modulus, Poisson's Ratio, and stress-strain curve models in MATPRO were used. Both elastic and plastic material models were used for comparison of mechanical response of unirradiated fuel bundles to large-deformation validation tests (Snell, 2007; Snell, 2009). However, for the case of spent fuel bundles resting in module tubes during dry storage, small deformations of the fuel elements less than 1-2 mm are expected and plastic deformation of the bundle is unlikely. Therefore, plastic material properties were not required for this analysis.

2.1.1 Zircaloy-4 Material Properties

A more recent version of MATPRO (MATPRO, 2003) was used for the elastic material properties of irradiated Zircaloy-4 (Zr-4). However, the elastic modulus model used in the two versions of MATPRO are identical. The elastic modulus (E) as a function of temperature (T) and fast neutron fluence (ϕ) is given in Pascals as,

$$E = \frac{1.088 \times 10^{11} - 5.475 \times 10^7 T}{0.88 + 0.12e^{-\phi^{10^{-25}}}},$$

where the temperature is in Kelvin and the fluence in neutrons per meter squared.

The fast neutron fluence was estimated from reactor physics codes. The approximated value used in this analysis for the fluence was $3 \times 10^{24} \text{ m}^{-2}$. The initial dry storage fuel temperature of 130°C was also used to define the elastic modulus. Table 1 summarizes the elastic modulus values for irradiated and unirradiated fuel bundles at room temperature and the initial dry

storage temperature. As can be seen from the table, neutron irradiation acts to increase the elastic modulus while temperature decreases it. The net result in moving from unirradiated Zr-4 at room temperature to irradiated Zr-4 at 130°C is a 5% drop in the elastic modulus.

The Poisson Ratio used for irradiated Zr-4 is not given in MATPRO and the best estimate value determined from the bundle model sensitivity study (Popescu and Lampman, 2009), 0.36, was used.

Table 1: Zircaloy-4 Elastic Modulus Values

Temperature (K)	Fast Neutron Fluence (m ⁻²)	Elastic Modulus (GPa)
Room Temperature (273 K)	0	93.9
	3×10^{24}	95.3
Initial Dry Storage Temperature (403 K)	0	86.7
	3×10^{24}	89.5

2.1.2 Uranium Dioxide Material Properties

The elastic modulus of the stoichiometric UO₂ pellets is given in MATPRO (MATPRO, 2003) as a function of temperature (T) and density fraction (D) as,

$$E = 2.334 \times 10^{11} [1 - 2.752(1 - D)] [1 - 1.0915 \times 10^{-4} T]$$

where the density fraction is the pellet density divided by the theoretical density for UO₂ of 10.98 g/cm³. The elastic modulus is given in units of Pascals.

The density of fuel pellets changes slightly with irradiation due primarily to two processes. The generation of fission products in a gaseous phase act to increase pellet porosity and reduce density. Opposing this is additional sintering of the pellet due to the high operating temperatures. The temperature gradient across a fuel pellet during operation is large resulting in significant differences in microstructure and porosity. Therefore, the fuel pellet density is a complex function of irradiation time and is dependent on power histories.

Further to the bulk material property variances in irradiated fuel pellets, they also undergo cracking during irradiation. During bundle power increases, the pellets will form radial cracks near their outer surface. During bundle power decreases, such as during cooldown after discharge from the reactor, the pellets will form circumferential cracks. Therefore, an irradiated fuel pellet will have non-homogeneous material properties and will be partially cracked, depending on the pellet's power history.

Modelling the specific response of irradiated fuel pellets to mechanical loads provides a significant challenge with no known experimental evidence to support the models. However, the pellets are significantly stiffer than the Zr-4 structural material and a modulus of 216.5 GPa from the fuel bundle model sensitivity study (Popescu and Lampman, 2009) was used to illustrate this effect.

2.2 Spent Fuel Bundle Geometries

Spent CANDU fuel bundle profilometry was reviewed for this case study to evaluate the post-discharge geometry of spent CANDU fuel bundles. During Post-Irradiation Examinations (PIE),

examinations of intact bundles include profiling the shape of the entire bundle structure is performed. In addition, each element of the bundle is removed and a 3-dimensional profile of the element is measured and recorded. Typically, the "free-element" profile of an element is a simple bow with the greatest deflection found at the center of the element where the spacer pads are located. The fuel bundle models were designed with this typical profile in mind; the initial shape of the fuel elements can be created with a user-specified mid-element deformation in the plane perpendicular to the bundle axis. The remaining axial profile of the element is modelled as a half-sine wave. This is shown in Figure 2 illustrating the axial and side view of a modelled fuel element with initial deflection.

From the review of available profilometry data, the post-discharge geometry of two 28-element bundles were created for this case study. End views of a bundle with high burnup, 28A, and a bundle with a typical burnup, 28B, are shown in Figure 3 and Figure 4. A best-estimate of the bottom of each bundle determined from visual inspection is also illustrated in the figures. Bowing of the high-burnup fuel elements is clearly seen in bundle 28A and it appears as though the bundle has crept to the radial profile of the reactor pressure tube. The bowing of the typical-burnup fuel elements in bundle 28B is less obvious and may be due to its lower burnup and the amount of pressure tube creep in the fuel channel. Both of these initial fuel bundle geometries have been used in the current analysis.

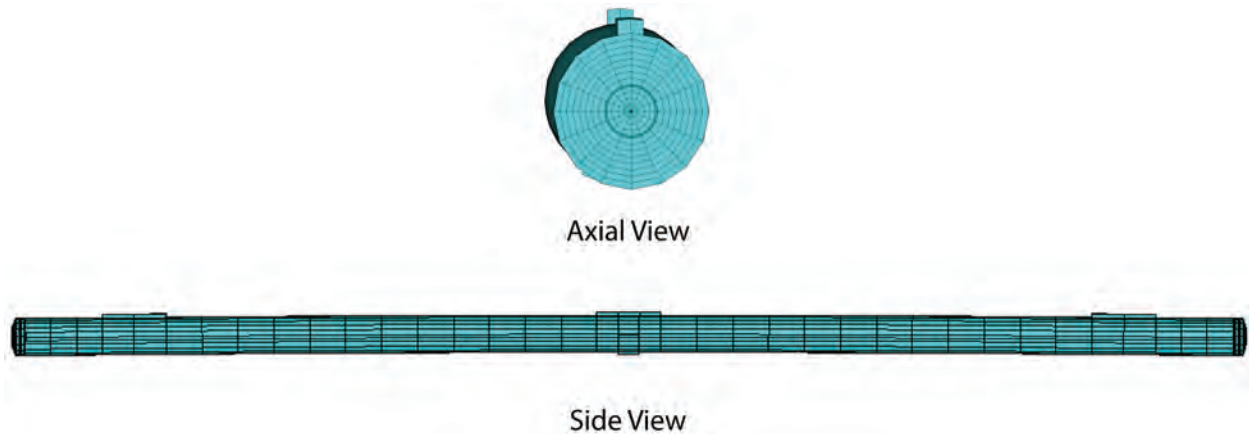


Figure 2: ANSYS Finite Element Model of a Bowed Fuel Element

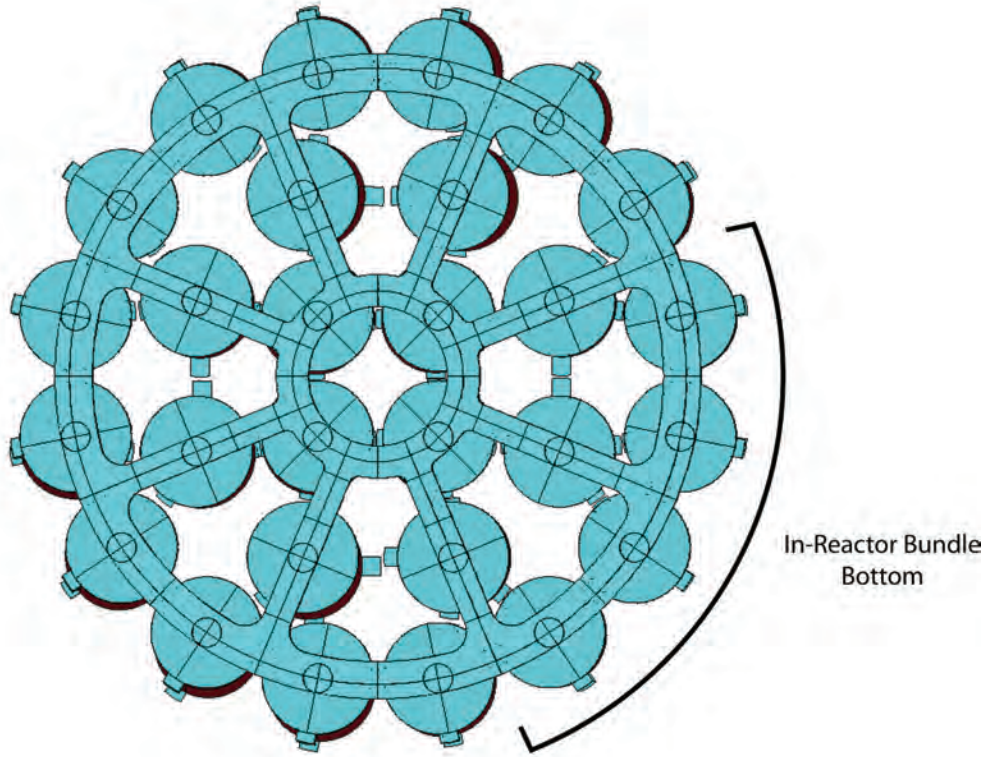


Figure 3: Initial Geometry of High-Burnup Bundle 28A

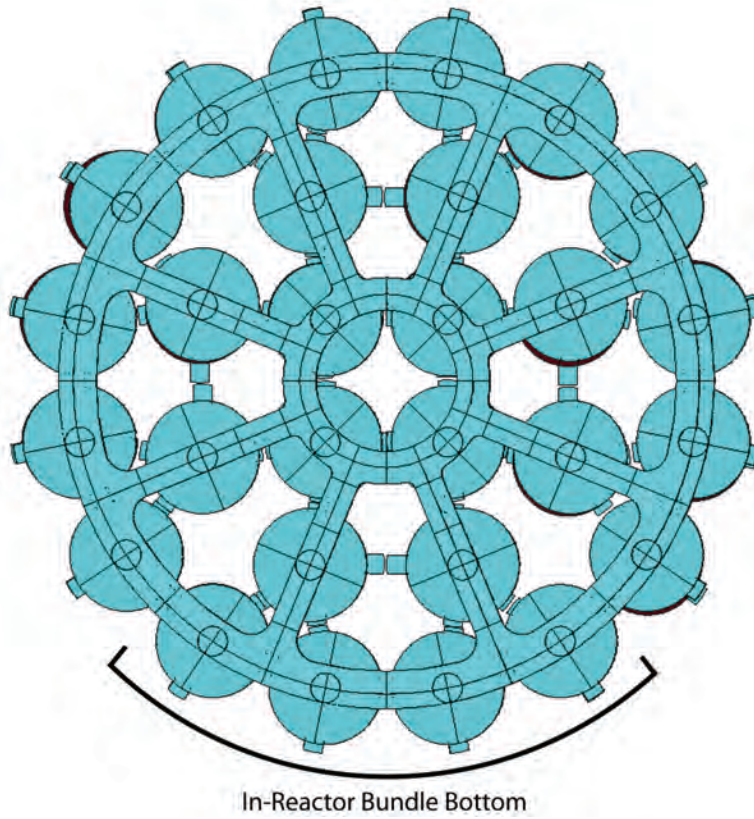


Figure 4: Initial Geometry of Average-Burnup Bundle 28B

2.3 Fuel Element Models

The CANDU fuel bundle models have been designed so that different fuel element models may be used and interchanged for each individual element in the bundle as desired. Currently, there are four different fuel element models: a *pipe model* where pipe finite elements are used to model the sheath and the mass of the pellets; a *hollow model* where the sheath is explicitly modelled using shell finite elements and the mass of the pellets are included; a *pellet contact model*, which is an extension of the hollow model with individual pellets and pellet-to-pellet and pellet-to-sheath contacts are modelled using contact and target surfaces; and the *pellet interface model* with individual pellets and the pellet-to-pellet and pellet-to-sheath contacts are modelled using interface finite elements².

The finite element models (Lampman *et al.*, 2009; Popescu and Lampman, 2009) used for the simulation of the 28-element fuel bundle have between 300,000 and 500,000 degrees of freedom, depending of the options used for the pellet-to-sheath interaction. The solution is obtained using a steady-state analysis; however, between 3 and 10 iterations are necessary to solve the geometrical non-linearities, *i.e.* to solve the contact status. The submodels employed to evaluate the stress intensity factor at the assembly welds have more than 200,000 degrees of freedom.

As mentioned previously, the fuel pellets will crack as a result of irradiation. In addition, the pellets' dimensions also change and are dependent on the power history of the fuel element. Measurements of irradiated pellet diameter have been made during PIE. However, due to pellet cracking and relocation, the measurements are not sufficiently accurate to be used for modelling purposes.

The selection of a fuel element model could have a significant impact on the response of the fuel bundle. A conservative approach regarding the fuel element model was taken. The hollow element does not contain the stiffening effect from the fuel pellet and is expected to have a larger bending magnitude for a given load when compared to a model accounting for pellet interactions. To confirm this expectation, a comparison of the irradiated hollow fuel element model and the irradiated interface model under identical loads and boundary conditions was performed.

2.3.1 Mechanical Loads for Comparison of Fuel Element Models

To perform the comparison of the fuel element models, the full 28-element fuel bundle model was used. The boundary conditions applied to the models is shown in Figure 5. The entire bundle was constrained by fixing the degrees of freedom (DOF) for the outer surface nodes of the central bearing pad of elements 9 and 16. A total external load of 100 N (approximately 40% of the bundle weight) was applied to the central bearing pad of element 5. The direction of the load was in the outward radial direction with respect to the bundle's axis. Gravitational forces were not included in the solution.

² The interface finite elements in ANSYS allow for the custom definition on the pressure between two opposing surfaces as the distance between the surfaces changes.

An evaluation of the different fuel element models was performed by changing the model for element 5. All remaining elements in the bundle were consistently modelled with the hollow fuel element model to reduce the overall size of the model.

2.3.2 Comparison of Fuel Element Models

ANSYS was used to solve the model with the two different fuel element models under the conditions described in Section 2.3.1. All simulations were performed with irradiated material properties at a temperature of 130°C. The hollow fuel element model simulation used the best-fit geometry determined from the unirradiated sensitivity studies (Popescu and Lampman, 2009). The irradiated interface element model also used the best-fit geometry with the exception that reduced pellet gaps were modelled to represent the effect irradiation appears to have on the fuel element response.

Experience from PIE is that the fuel pellets cannot be removed from irradiated fuel elements without force. Therefore, it is expected that the gaps between the fuel pellets and the sheath have reduced relative to the unirradiated fuel element. The effect of irradiation on the fuel element was simulated selecting virtually closed axial and radial pellet gaps.

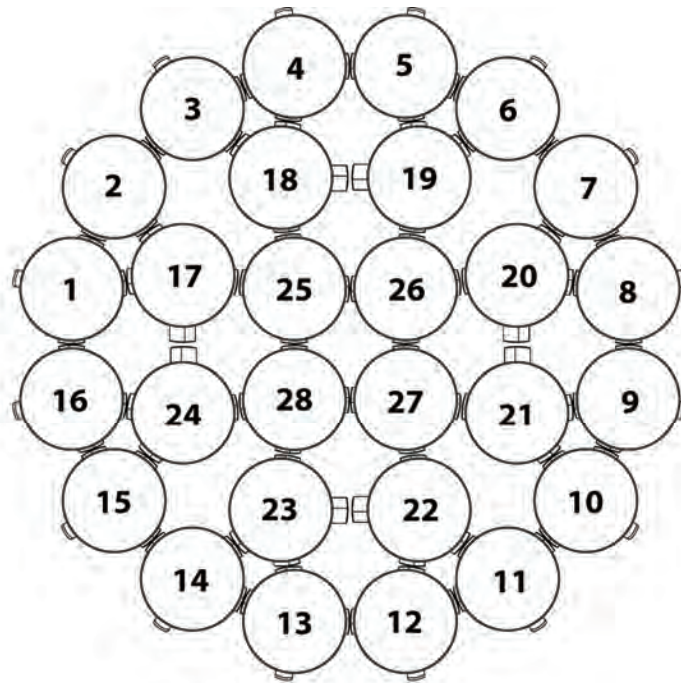
From each of the simulations, the maximum displacement of the central bearing pad on element 5 relative to the endplate was determined for comparison of the fuel element deformation. As well, the 28-element submodel of the assembly weld region was used to determine the maximum K_I value at the weld crack tip.

The geometry of the 28-element submodel is shown in Figure 6. The submodel consists of the endcap and a portion of the endplate surrounding the assembly weld region. The mesh used for the submodel is much finer than used in the full bundle model. In the welded region where the endcap connects to the endplate, a special mesh is created to include a sharp crack around the weld with a depth³ of 0.5 mm. Singular finite elements are created at the crack tip to facilitate for the calculation of K_I using the ANSYS crack tip displacement methodology. The submodel is used in the manner established by ANSYS:

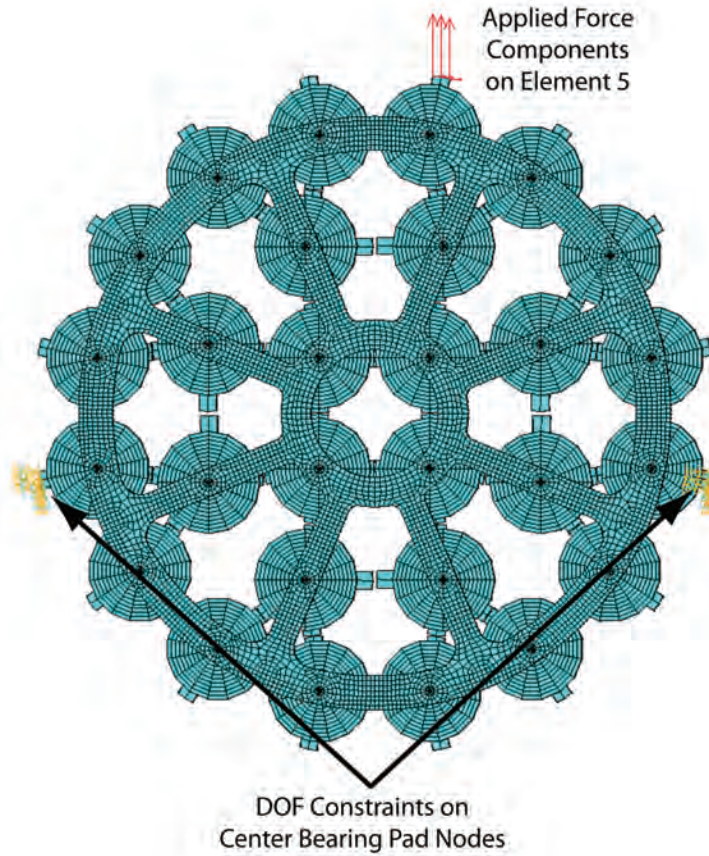
1. Create submodel mesh.
2. Define submodel cutting surfaces (illustrated in Figure 6) and determine nodes on the cutting surfaces.
3. Interpolate the displacements of the cutting surface nodes from the full-bundle model results.
4. Apply cutting surface node displacements to the submodel nodes.
5. Set environmental conditions in submodel to be equivalent to full-bundle model.
6. Solve and post-process.

The results of these calculations are given in Table 2.

³ The 0.5 mm crack was used as suggested from assembly weld cross sections created by the NWMO program to determine the critical stress intensity factor for DHC in unirradiated CANDU fuel bundle assembly welds (Shek and Wasiluk, 2010).



(a) Element Numbering Scheme



(b) Nodal Constraints

Figure 5: Fuel Element Model Comparison Loads and Boundary Conditions

The interface model with near closure of the pellet gaps gives significantly less deflection of the element and a lower K_I value at the assembly weld. Because of the uncertainty in the irradiated fuel element geometry, the accuracy of the predictions is not qualified. However, the calculation represents a boundary case that delimits the range of possible responses of a fuel element subjected to a mechanical load. The results illustrate that the hollow fuel element model can be used in a conservative manner to generate larger element deflection to bending loads resulting in higher stress intensity factors at the assembly welds. It is expected that these values will be higher than in reality since the irradiated pellet will stiffen the element, as is observed from the predictions obtained from the pellet interface model.

Table 2: Comparison of Fuel Element Models under Bending Loads

Fuel Element Model	Mid-Element Deformation (mm)	Maximum K_I ($\text{MPa m}^{1/2}$)
Hollow Fuel Element	4.10	9.68
Pellet Interface Model	2.48	4.89

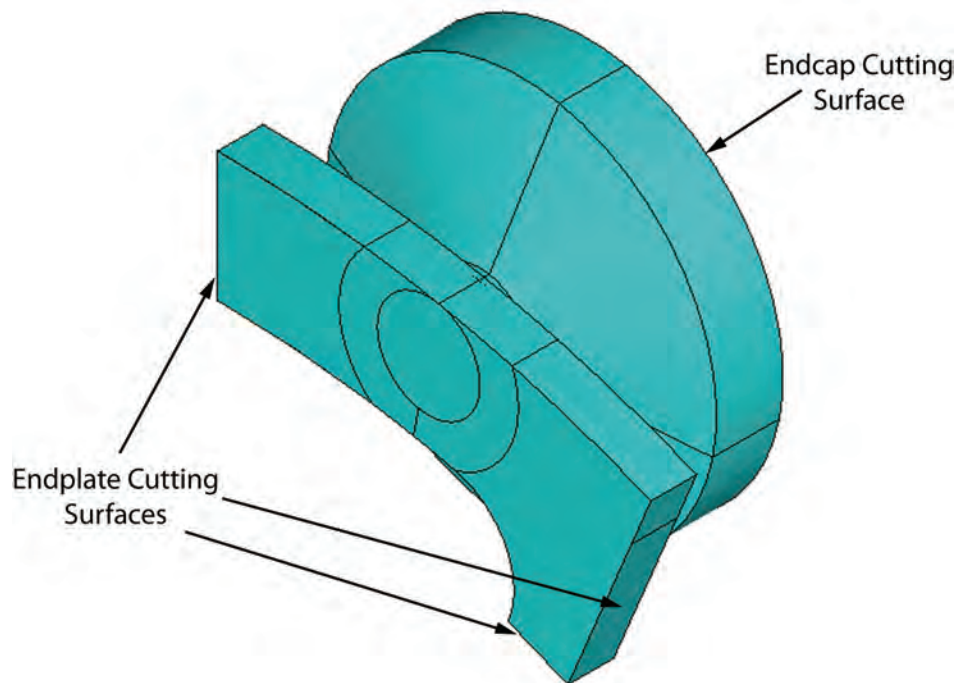


Figure 6: 28-Element Outer Ring Element Submodel Geometry

3. ANALYSIS OF SPENT CANDU FUEL BUNDLES DURING DRY STORAGE

A survey of the condition of all 1.5 million discharged CANDU fuel bundles from Pickering NGS, Darlington NGS, and Bruce NGS up to the end of 2004 has been performed (Lazaroski *et al.*, 2005). The study identified two basic populations of fuel from the total discharged population: the *bulk* population and the *segregated* population. The bulk population contains the large majority of all discharged fuel. The segregated population consists of fuel bundles that have been physically separated from the bulk population for various reasons specific to each nuclear generating station. For this report, analysis of the segregated population stress levels was not performed.

In the bulk population stresses in the endplate will be affected by two factors. All fuel bundles placed in OPG's DSC will experience stress due to gravitational loading. Bending of the horizontal fuel elements will affect the stress levels around the assembly weld cracks. Ageing of the reactor fuel channels is resulting in increased sag and diametral creep of the pressure tube. Discharged bundles appear to be affected by the fuel channel profile, which could lead to increased stress levels in the endplates due to bundle bowing. An additional source of endplate stress could come from any atypical fuel conditions, such as mechanical damage to the bundles from reactor components. The 2005 Study by Lazaroski *et al.* identified atypical fuel conditions from visual fuel bundle inspection results that could potentially affect endplate stress levels.

This section presents the results of finite element analyses performed to evaluate the stress developed in endplates of the bulk population due to bundle geometry effects on 28-element fuel bundles. Section 3.1 evaluates the stress distributions and assembly weld K_I values for CANDU fuel bundles discharged with fuel element bowing within typical observed ranges. Three bundle geometries were evaluated: a nominal geometry with no bowing, an average-burnup bundle geometry, and a high-burnup bundle geometry. Section 3.2 evaluates the stress distributions and assembly weld K_I values for a proposed geometry of a bundle discharged from a crept fuel channel. Section 3.3 discusses the affect the atypical fuel conditions identified in the Lazaroski *et al.* report may have on spent fuel stress levels.

3.1 Typical Fuel Bundle Geometry Stress Distributions

The 2005 Study by Lazaroski *et al.* indicated that the majority of spent fuel in the bulk population does not show any indication of atypical deformation or damage that could in itself increase the stress levels at the assembly welds. The assembly weld stress levels in this fuel would originate mainly from residual stresses due to the manufacturing, stress present from the post-discharge geometry of the fuel, and induced stress from gravitational forces on the fuel in the module tubes of a DSC.

The residual stresses in the assembly welds from manufacturing of CANDU fuel bundles are not well understood. Initial results from simulations of the welding process on CANDU fuel suggest that stress levels around the weld crack in unirradiated bundles may be as high as several hundred MPa. However, these estimated high stresses are conservative bounding values since the effects from creep-induced stress relaxation were not considered. The neutron flux and operating temperature during the average one-year in-core residence time of a bundle are expected to significantly reduce the high initial residual stress levels that may exist. It is assumed for this work that the residual stresses from manufacture are insignificant to

elastic loads during dry storage. However, this currently isn't clearly understood and further work to validate this assumption is recommended.

Stresses arising from the post-discharge geometry of the bundle have been evaluated with the stress model using normal-burnup and high-burnup profiles. The resultant stress once these fuel bundles are placed in module tubes was performed. For comparison, the stress resulting from a nominal bundle geometry without initial bowing of elements has been evaluated and reported. The fuel element numbering scheme presented in Figure 5(a) is applicable to all analyses presented.

3.1.1 Spent Fuel Bundle Geometries

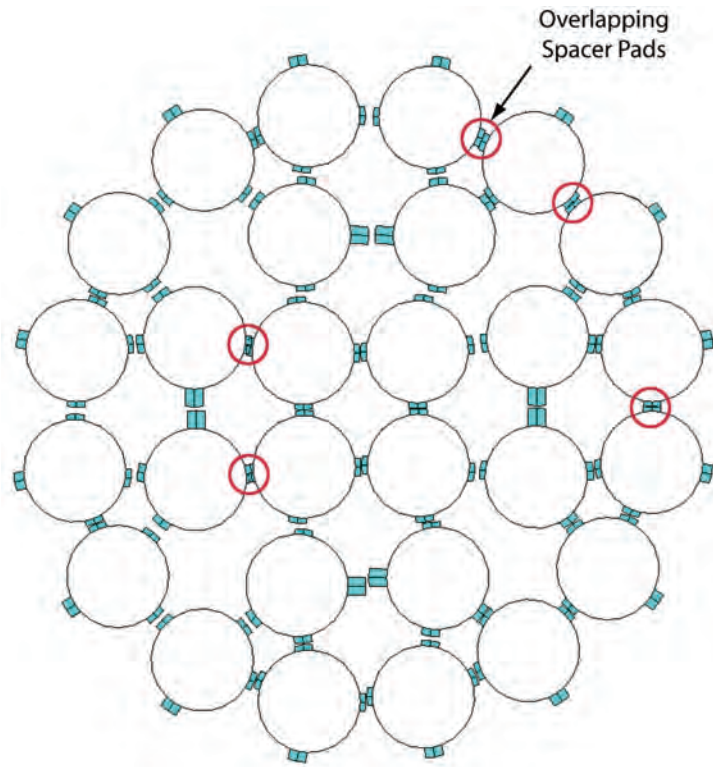
The unconstrained, single-element PIE profilometry results were used to evaluate endplate stresses and associated stress intensity factors at the assembly weld crack. The post-discharge geometry in the fuel bundle models were created from the PIE results. When fuel elements profiles are modeled in the full bundles, the resulted assemblies have several spacer pad pairs overlapping. This can be seen in Figure 7(a) and Figure 7(b) for bundles 28A and 28B, respectively. This interaction may result from relaxation of residual stress due to cooling of fuel bundles after discharge from the reactor.

To determine the stress distributions in the endplate and at the assembly welds resulting from spacer pad interaction, the post-discharge geometries were solved in ANSYS under zero external mechanical loads and gravitational acceleration. The solution prevented the overlapping of spacer pads, resulting in bending of elements and generation of stress in the endplates. The solution was performed at a temperature of 130°C. The hollow fuel element model was used for each element in the bundle.

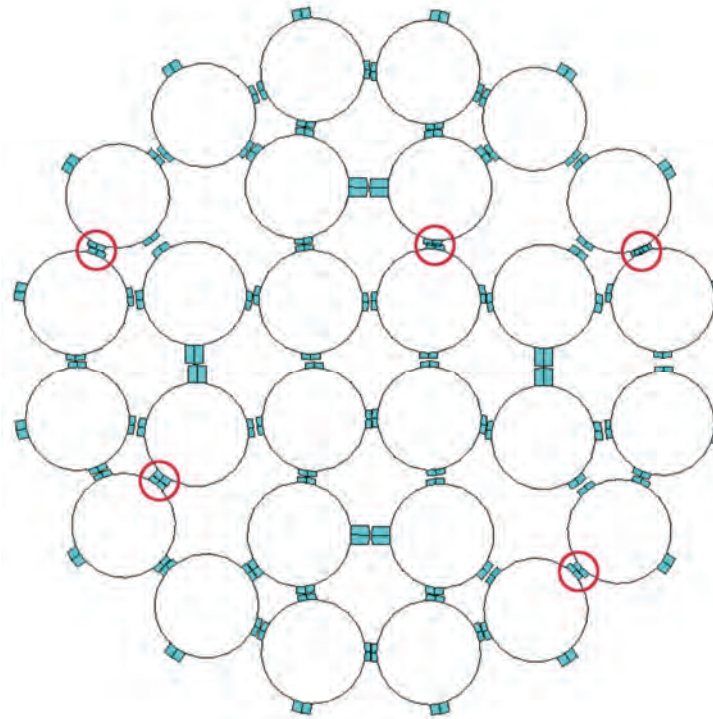
Figure 8 illustrates the resultant displacement of the fuel elements in the bundle mid-planes of the two bundles. The spacer pad overlap has been eliminated and displacements of the elements with overlapping spacers experience the greatest bending. In some cases, neighbouring elements are also affected, depending on the separation of spacer pads. The translation of the element bending to the stress distribution in the endplates can be seen in Figure 9 and Figure 10. Figure 9 illustrates the von Mises stress on the inside surface of the endplate facing the elements. The maximum stress is seen in the vicinity of the assembly welds for the elements with the maximum displacement.

Figure 10 illustrates the axial component of the stress field on the inside surface of the endplate. The axial stress extreme values are seen at the assembly welds. It can be seen that one side of the weld is under compression (negative axial stress) and the opposite side in tension (positive axial stress) which is consistent with the bending of the elements. The maximum axial stress in bundle 28B, 28 MPa, is double that seen in bundle 28A, 13 MPa. To calculate the stress intensity factors at the assembly weld cracks, the 28-element submodel was used.

The submodel was run for several assembly welds on each bundle. The element with the maximum tensile stress was examined, along with several outer-ring elements. The results of the submodel calculations are shown in Table 3. The K_I value in the table corresponds to the value calculated at the weld tip region with the maximum tensile strain. The results suggest that critical stress intensities as large as $1.5 \text{ MPa m}^{1/2}$ may be present in spent 28-element CANDU fuel due solely to the post-discharge geometry of the bundle, prior to any loading due to storage.

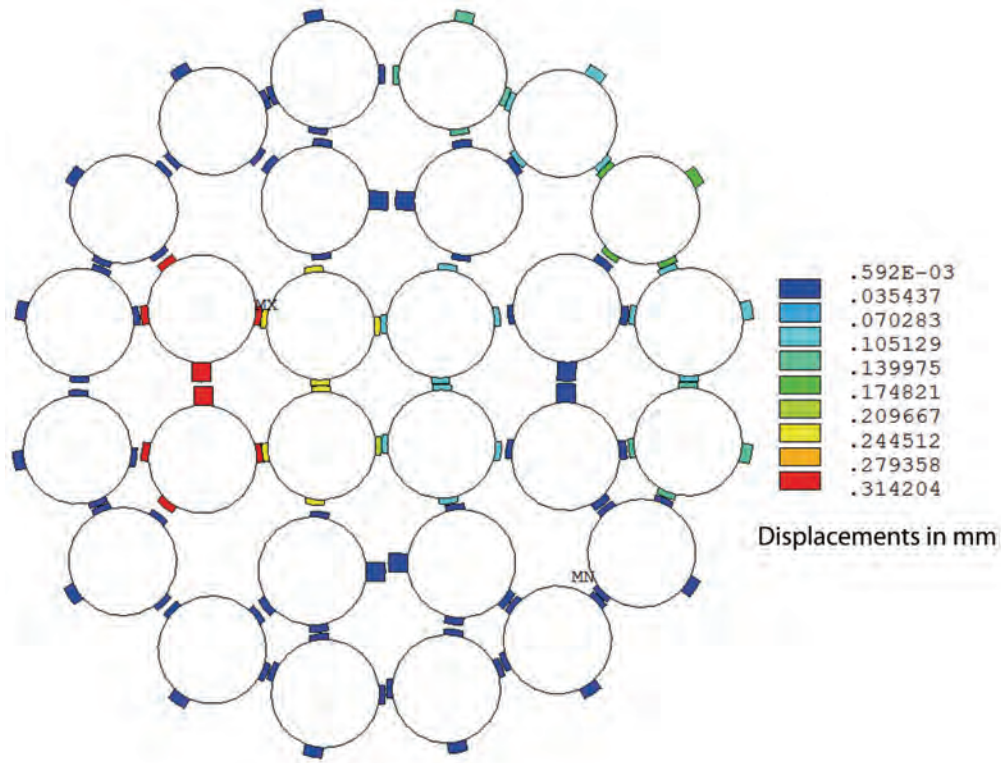


(a) Bundle 28A

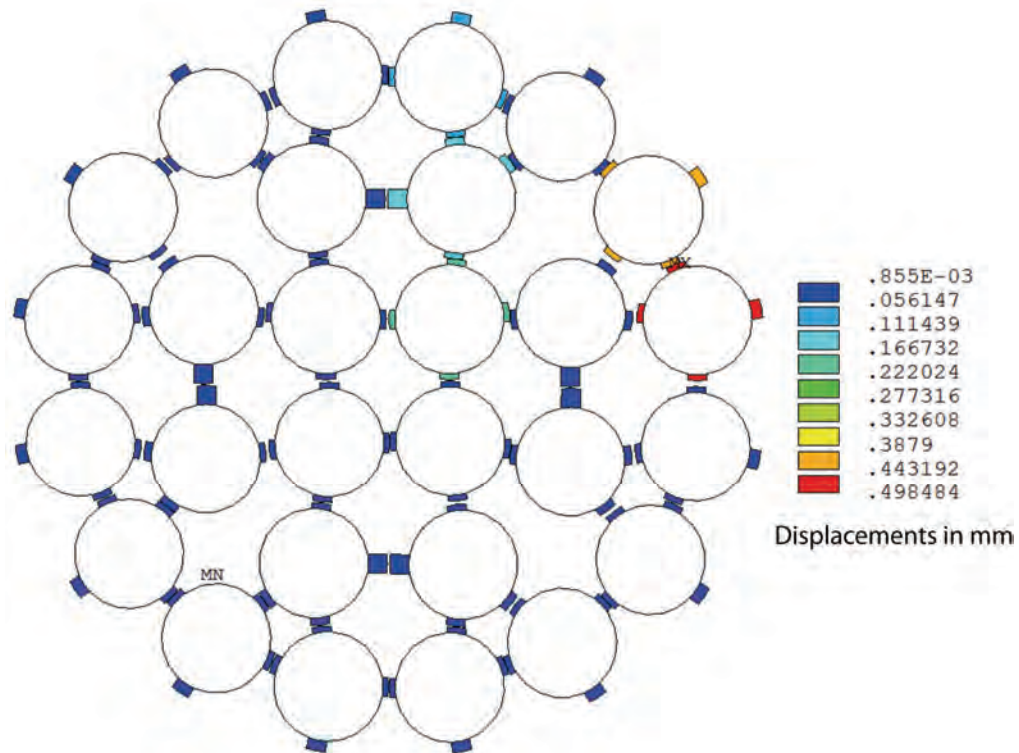


(b) Bundle 28B

Figure 7: Mid-Bundle Cross Section of Post-Discharge 28-Element Bundle Geometry



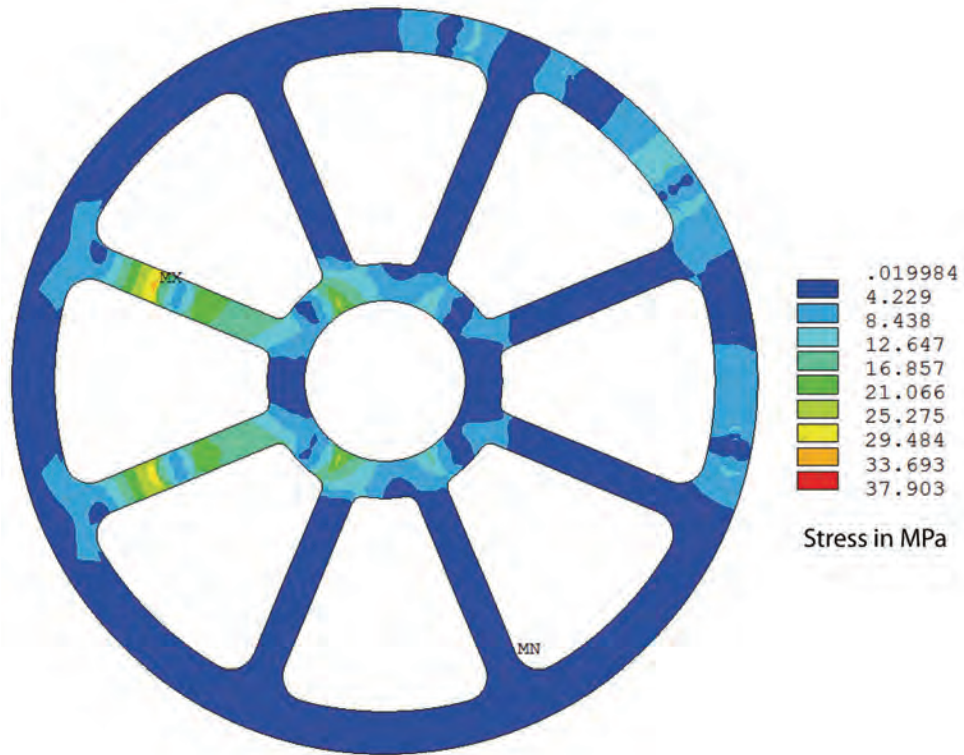
(a) Bundle 28A



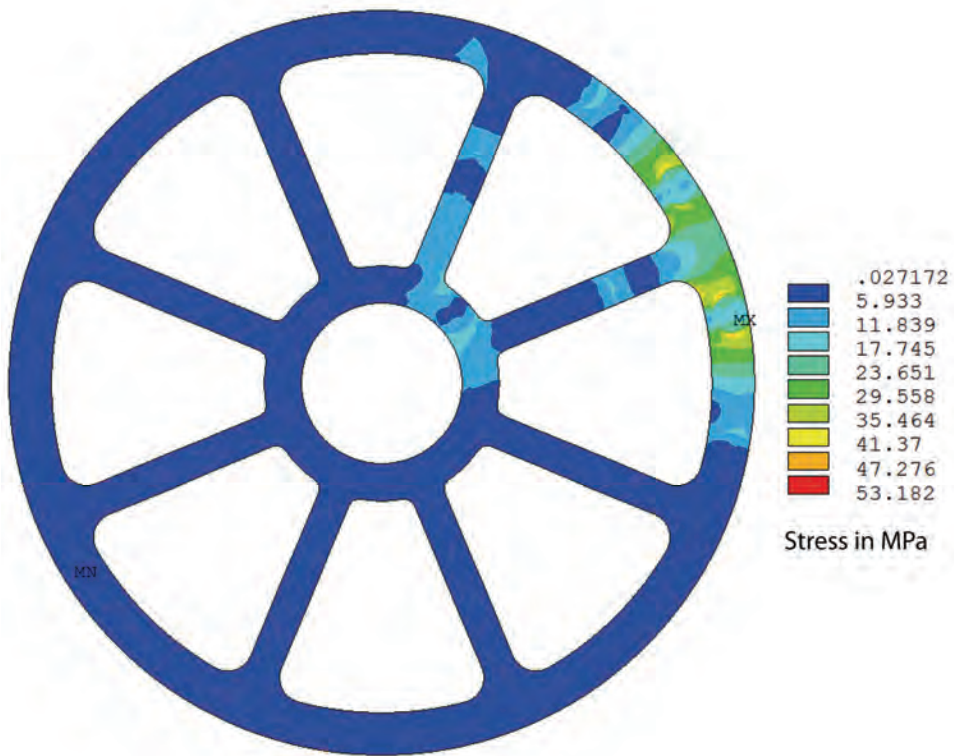
(b) Bundle 28B

Figure 8: Total Displacement of the Fuel Elements at the Bundle Mid-Plane

Note: The ANSYS postprocessor places the labels MN and MX on the contour plots to identify the location of the minimum and the maximum values of the results.



(a) Bundle 28A



(b) Bundle 28B

Figure 9: Endplate von Mises Stress Distribution Due to Post-Discharge Geometry

Table 3: Post-Discharge Assembly Weld Maximum Stress Intensity Factors for a Crack Depth of 0.5 mm

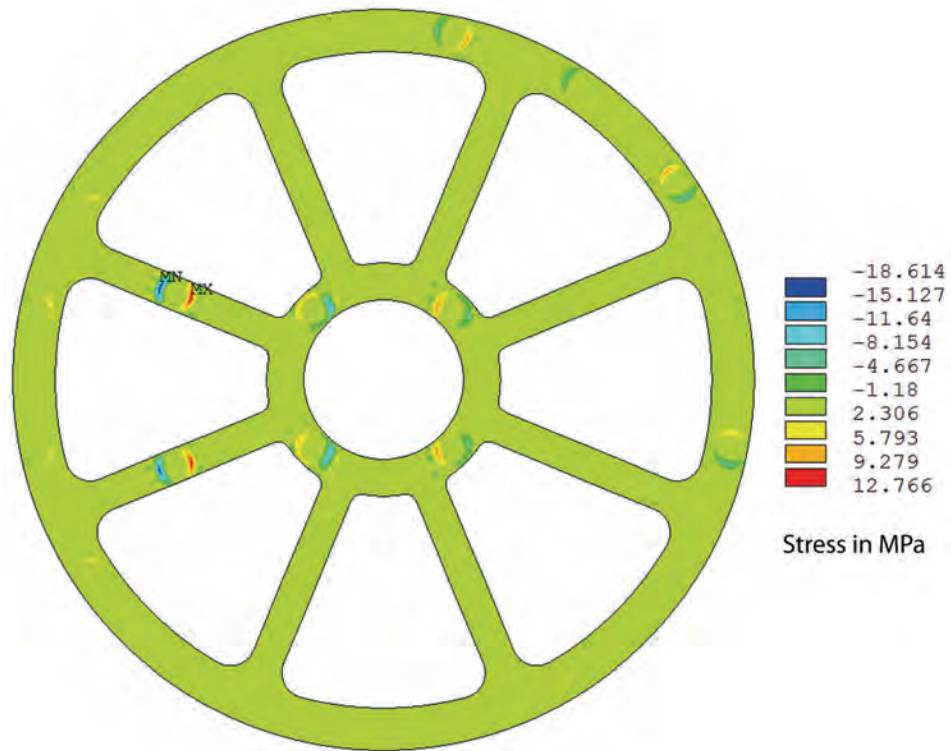
Bundle	Element	K_I (MPa m^{1/2})
28A	7	0.40
	9	0.30
	17	0.83
28B	7	1.16
	8	1.48
	20	0.09

3.1.2 Nominal Fuel Bundle in a Module Tube

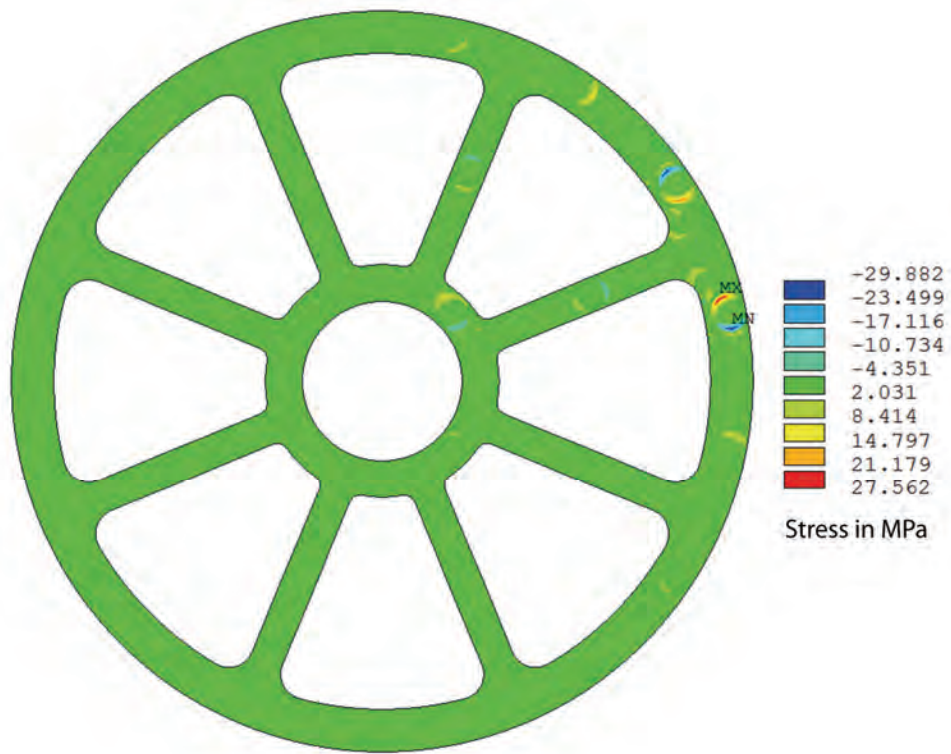
The stress distribution resulting from a bundle with no initial element bowing placed horizontally in a module tube was calculated using the CANDU fuel bundle model. The geometry of the system to model is shown in Figure 11. The temperature of the simulation is the approximate initial expected fuel sheath temperature of 130°C. The module tube is not explicitly modelled in ANSYS as this would require additional contact pairs further complicating convergence of the solution. Instead, the contact of bearing pads with the module tube is modelled through the application of constraints on the bearing pad nodes representing module tube contact.

The approach taken to model the contact with the module tube is as follows:

1. Create the full bundle model and constrain the bearing pad nodes known to contact the module tube.
2. Apply gravitational loads and solve the model.
3. Post-process the solution data to determine the resulting displacement of each bearing pad surface node.
4. Evaluate which nodes penetrate into the module tube. For each of these nodes, determine a scaling factor the displacements which would move the node in contact with the module tube.
5. Constrain the nodes penetrating the module tube to the inner surface of the tube. The spatial components of the constraint are determined from the scaling factor. In some cases, penetration is minor (the scaling factor is nearly equal to 1) and a constraint is not applied.
6. Re-solve the model.
7. Repeat steps 3 to 6 until no nodes penetrate the module tube.



(a) Bundle 28A



(b) Bundle 28B

Figure 10: Endplate Axial Stress Distribution Due to Post-Discharge Geometry

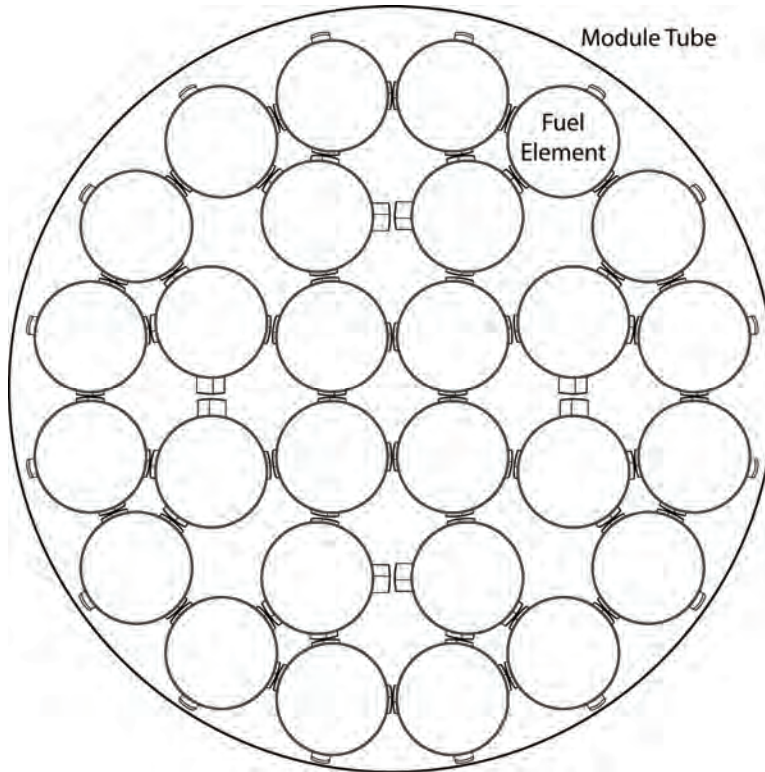
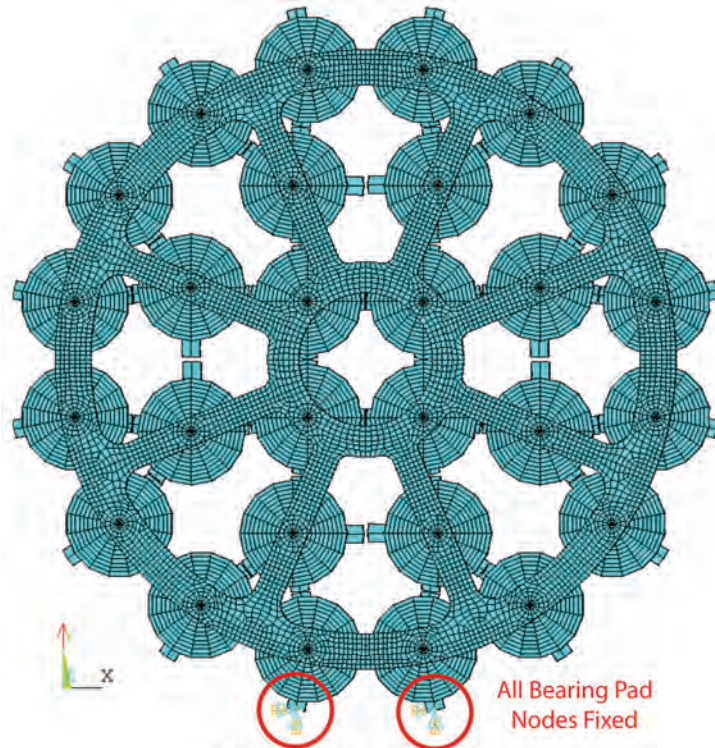


Figure 11: Cross Section of a 28-Element Fuel Bundle in a Module Tube

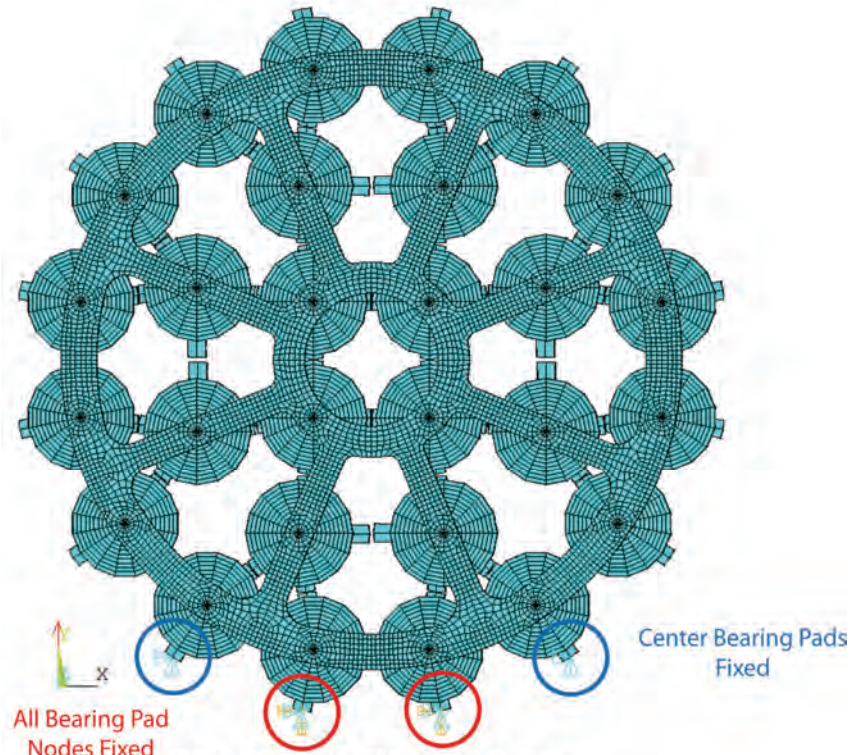
The initial model conditions are shown in Figure 12(a) where a gravitational acceleration of 9.8 m/s^2 is applied in the negative y -direction. The surface nodes on all bottom element bearing pads (elements 12 and 13) are constrained with zero displacement along the x - and y -axes. The central nodes on the two center bearing pads are also constrained to zero displacement along the z -axis to prevent rigid body motion.

After the first iteration, the central bearing pad nodes on the elements adjacent to the bottom elements (elements 11 and 14) contact the module tube, as shown in Figure 12(b). Solving the model with the updated constraints did not produce any additional nodes that penetrated the module tube, so the solution to the system in Figure 12(b) was used to evaluate the stress distribution in the 28-element fuel bundle.

The total displacement of the elements in the bundle mid-plane is shown in Figure 13. It can be seen in the figure that the minimum displacement is seen at the bottom of the bundle. The elements in this region are supporting the weight of the bundle. The maximum displacement is seen in the top four outer-ring elements and the four side intermediate-ring elements. The von Mises stress on the inner surface of the endplate is shown in Figure 14(a). The maximum stress is on the connection between the radial endplate arms and the inner ring. In terms of stress magnitudes in the assembly weld regions, the maximum is seen for the bottom two elements which support a majority of the bundle's weight. However, the axial component of the stress is relatively minor compared to the other elements, as seen in Figure 14(b), suggesting lower stress intensity factors.



(a) Initial Model Constraints



(b) First Iteration Model Constraints

Figure 12: Nodal Constraints Applied to Model to Simulate Contact with Module Tube

The 28-element submodel was used to determine the maximum K_I value at the assembly weld cracks of several elements. The results of the submodel calculations are given in Table 4. The stress intensity factor for element 12 at the bottom of the bundle was the smallest of the elements examined. Element 10 had the largest axial tensile stress and produced the largest K_I value of $1.01 \text{ MPa m}^{1/2}$. The inner-ring element 18 at the top of the bundle also gave a very similar K_I value.

Table 4: Calculated Assembly Weld Maximum Stress Intensity Factors for a Nominal 28-Element Bundle in a Module Tube

Element	K_I ($\text{MPa m}^{1/2}$)
8	0.90
10	1.01
12	0.44
18	0.97

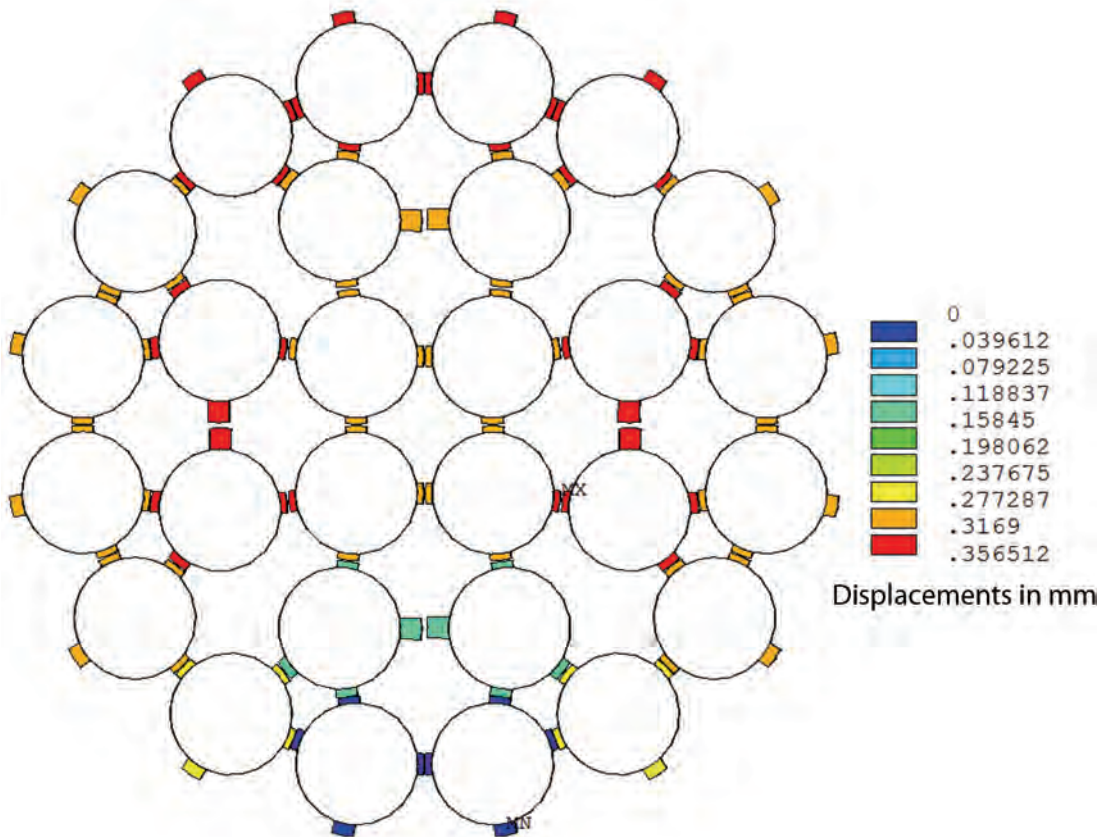
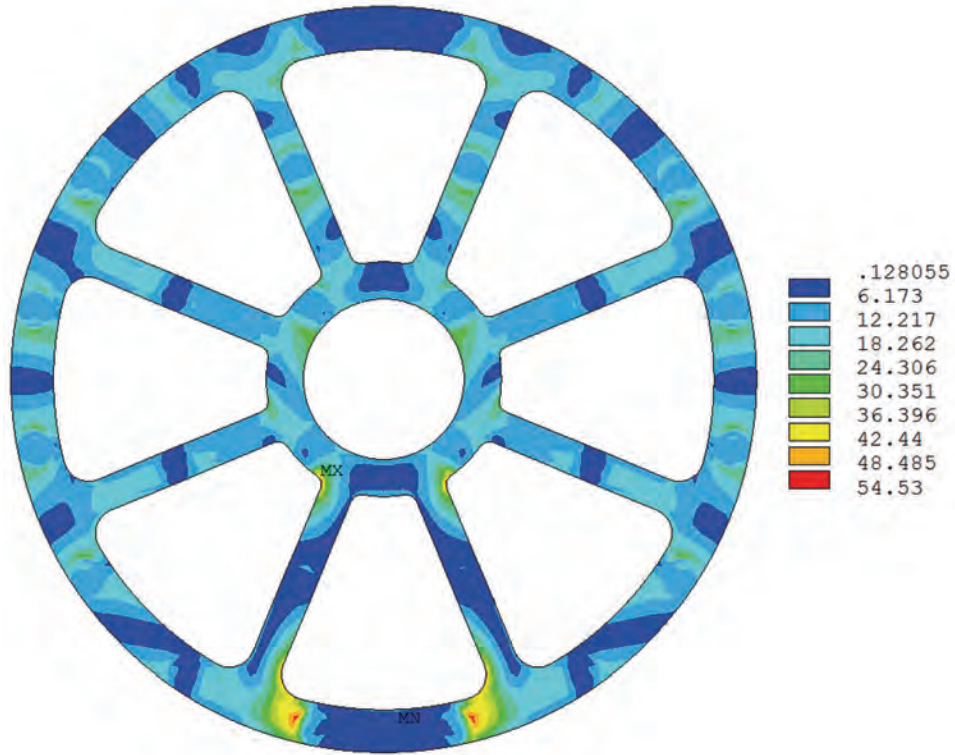
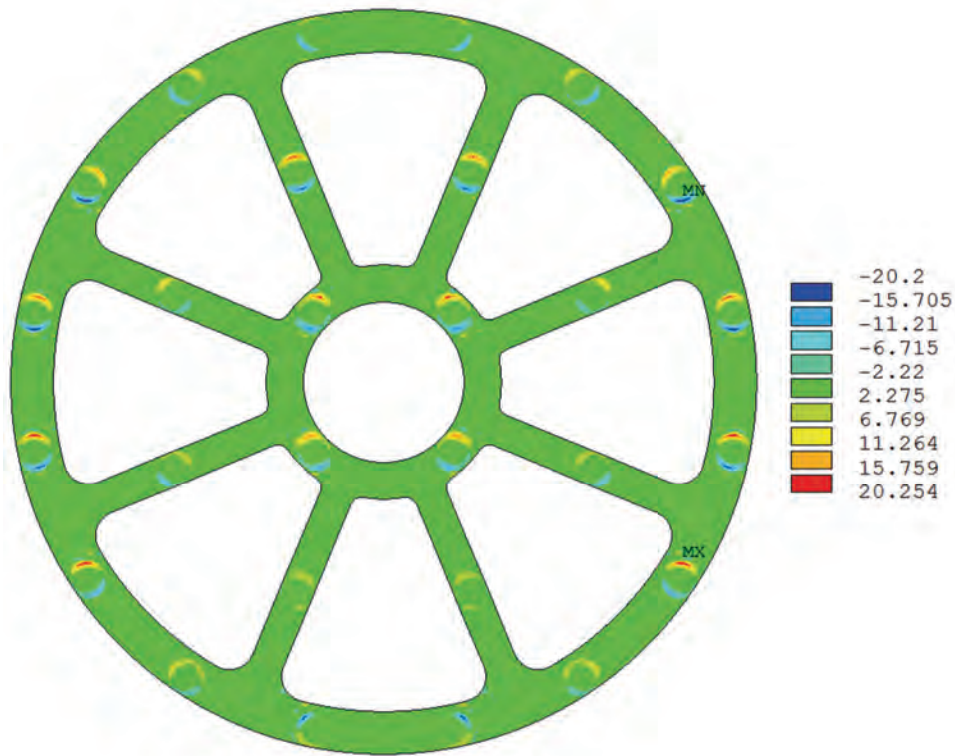


Figure 13: Total Displacement of the Fuel Elements in the Bundle Mid-Plane



(a) von Mises (MPa)



(b) Axial Component (MPa)

Figure 14: Stress Distribution in the Endplate of Nominal Bundle in a Module Tube

3.1.3 Spent Fuel Bundle in a Module Tube

A mechanical analysis was performed using the geometry of the normal-burnup bundle, bundle 28B in Figure 7(b), supported in the module tube under gravitational acceleration. The acceleration is applied parallel with y-axis (vertically in the presented figures). The temperature of the simulation is the approximate initial fuel sheath temperature of 130°C.

The approach taken to model the contact between the bundle and the module tube is as follows:

1. Create the full bundle model using the geometry obtained from profilometry measurements. The middle bearing pads of two outer fuel elements located at the lowest position in Y direction (bottom of the bundle) were considered to be in contact with the support tube.
2. Apply gravitational loads in successive steps and solve the model for each step. Each step added 10% of the nominal gravitational acceleration.
3. For each load step, post-process the solution data to determine the resulting displacement of each of the bearing pads outer nodes.
4. Evaluate which nodes contacted the module tube. For each of these contacting nodes, restrain the movement in X, Y, and Z direction for subsequent load steps.
5. If 100% of the gravitation acceleration was applied, stop the calculations and go to step 6; if not, repeat from step 2 for the next load step.
6. Evaluate K_I using the finite element submodel for the assembly welds.

The small load steps used to apply the gravitational forces assure that the contacts between bearing pads and the module tube which support the bundle were correctly assessed. According to the current analysis methodology, the DOFs of any nodes penetrated the module tube were constrained for further load steps.

The results from the final load step, which correspond to 100% gravitational acceleration, are presented in Figure 15. The nodes which were predicted in contact with the module tube are marked. Because of the bundle geometry, the bearing pads contacting the module tube are not symmetrically distributed against the vertical plane. In addition, more bearing pads from the middle of the bundle are in contact to the module tube than pads located at each end of the bundle, which is consistent with previous analysis performed for a nominal bundle supported in a module tube.

The von Mises stress on the inner surface of the endplate is shown in Figure 16(a). The maximum stress was predicted in the vicinity of the assembly weld for element 8. The axial component has the maximum values predicted for the same weld, as seen in Figure 16(b). The maximum values of the stress intensity factors at the assembly weld cracks of several elements were evaluated using the 28-element submodel, and are summarized in Table 5. The highest value for the stress intensity factor is 2.45 MPa m^{1/2} for element 8. For comparison, the stress intensity factor for a fuel element located at the bottom of the bundle, element 12, is 0.80 MPa m^{1/2}.

Table 5: Calculated Assembly Weld Maximum Stress Intensity Factors for an Average-Burnup 28-Element Bundle in a Module Tube

Element	K_I (MPa m ^{1/2})
8	2.45
12	0.80

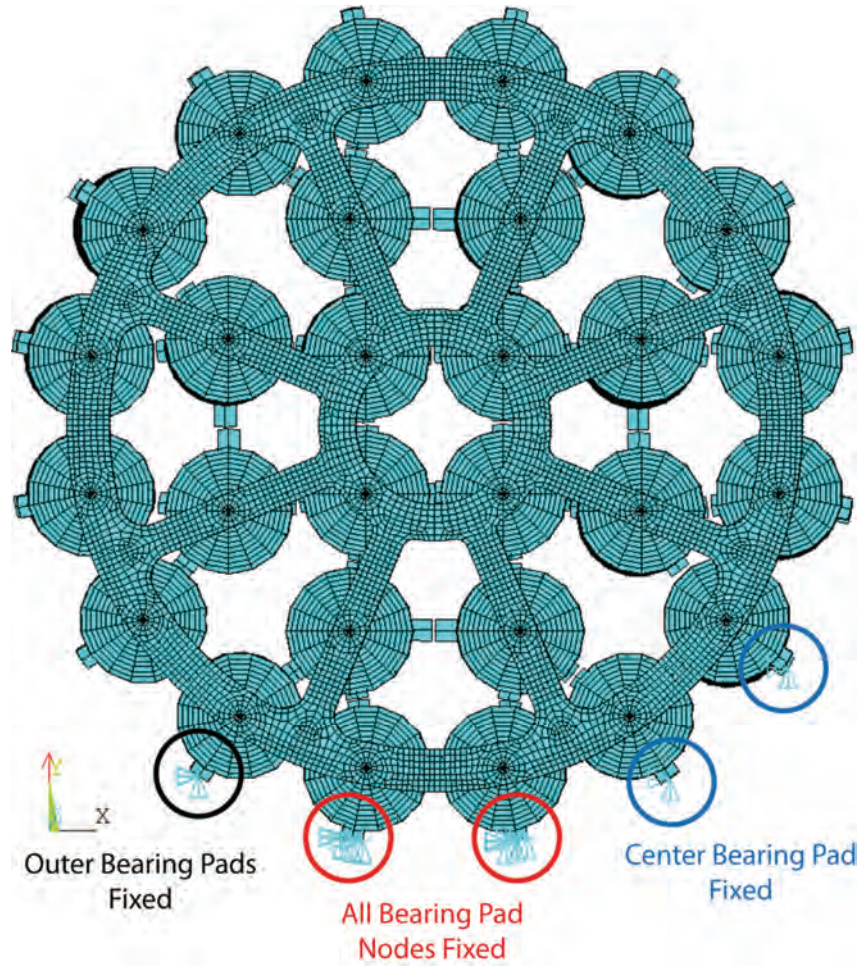
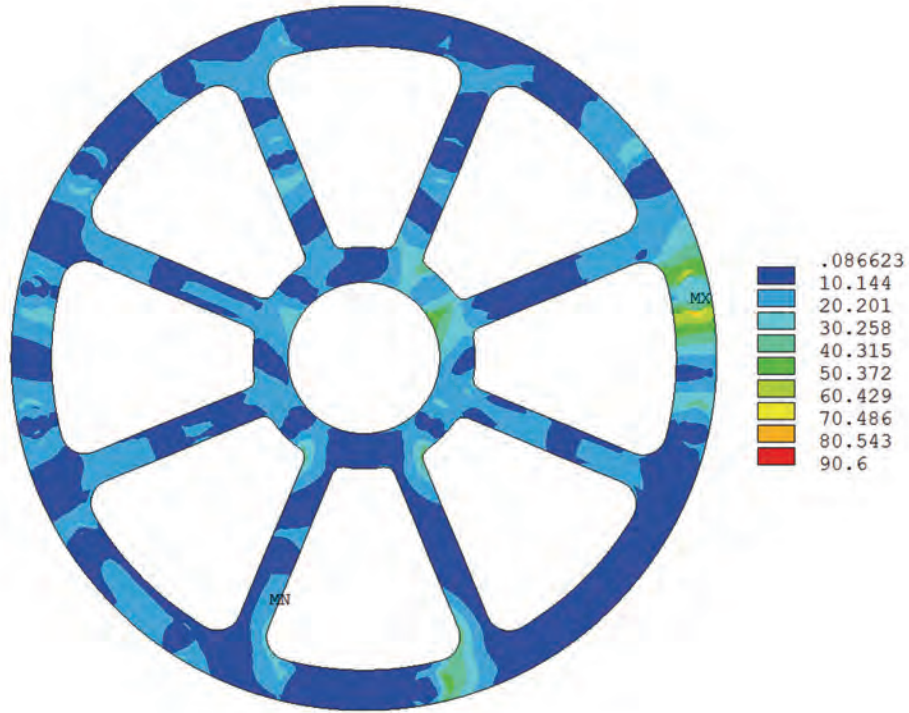
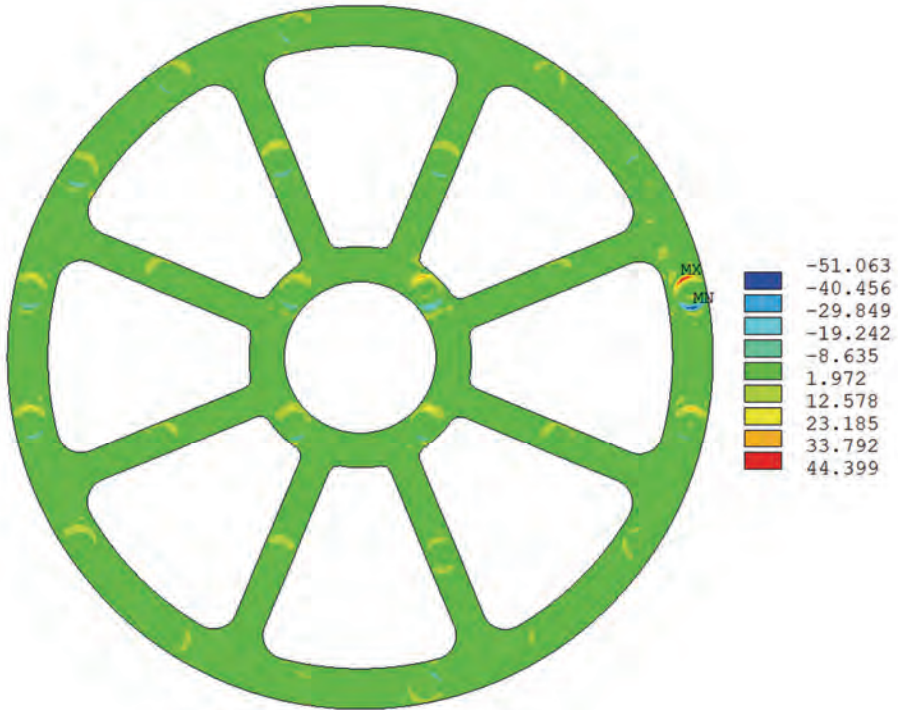


Figure 15: Nodal Constraints to Model the Module Tube for an Average-Burnup Bundle Geometry



(a) von Mises (MPa)



(b) Axial Component (MPa)

Figure 16: Stress Distributions in the Endplate for Average-Burnup Bundle in Module Tube

3.2 Crept Channel Fuel Bundle Geometry Stress Distributions

With time, the fuel channels in the nuclear reactors are creeping due to the high operating temperatures and neutron flux. This is resulting in diametral creep of the pressure tube to larger diameters as well as vertical sag of the channel. The effect that the sag of a fuel channel might have on a fuel bundle is being assessed. However, while PIE examinations indicate bundles are slightly bowed as a result of irradiation, for the purpose of this study, it has been conservatively assumed that bundles take on a profile exactly matching a crept fuel channel profile.

The current sag profiles of several channels expected to have the largest amount of creep were reviewed to determine a potential range of bundle bowing. The profiles were broken down into separate profiles for each bundle location in the channel under the assumption that the bundle profile would match the channel profile. The bundle profiles all exhibited simple bowing with the maximum bow at the center of the bundle. The maximum bundle bow observed was less than 0.8 mm at the point of maximum bow deflection. A fuel bundle with this degree of bowing resting in a module tube was modelled using the fuel bundle model. Similar to the previous simulations, gravitational forces were modelled and the simulation temperature was 130°C.

The bowed bundle in a straight module tube was modelled by employing a straight bundle in a tube with the opposite profile of the bowed bundle, as shown in Figure 17, to allow for a better representation of the bundle bow profile. The analysis process is identical to the method described in Section 3.1.2. However, when evaluating which bearing pads nodes penetrated the module tube, consideration for the axial position along the bundle, and therefore the amount of bending of the module tube, was made. Two iterations were required to establish all nodes on the surface of the module tube. The first iteration only considered contact of the center bearing pad nodes for the two bottom elements, as shown in Figure 18(a). For the second iteration, all the bearing pads for the bottom four elements and the center bearing pads of the adjacent two elements were in contact with the module tube, as shown in Figure 18(b).

The displacement of the bundle is shown along the bundle axis in Figure 19 and on a side view in Figure 20. The endplates of the bundle drop approximately 0.89 mm. The majority of the bending occurs in the bottom two elements. The weight of the bundle is mainly carried up vertically through the center of the bundle and some deflection of the inner ring elements above the bottom elements is seen. The von Mises stress on the inner surface of the endplate is shown in Figure 21(a). The maximum stress is seen in the assembly weld region of the bottom two elements. The other outer-ring elements in contact with the module tube and the two intermediate-ring elements above the bottom two outer-ring elements also have reasonably enhanced stresses. The axial component of the stress field is shown in Figure 21(b) and indicates the maximum bending is predicted in the intermediate-ring elements.

Based on the axial component of the endplate stress field, the submodel was used to calculate the maximum K_I values at the crack tip in elements 11, 12, and 22. The results are given in Table 6. A maximum stress intensity factor of $3 \text{ MPa m}^{1/2}$ was calculated in element 22. The maximum stress intensity factor for an outer-ring element was $1.5 \text{ MPa m}^{1/2}$, which is not different than the maximum K_I calculated from the post-discharge geometry of a 28-element fuel bundle.

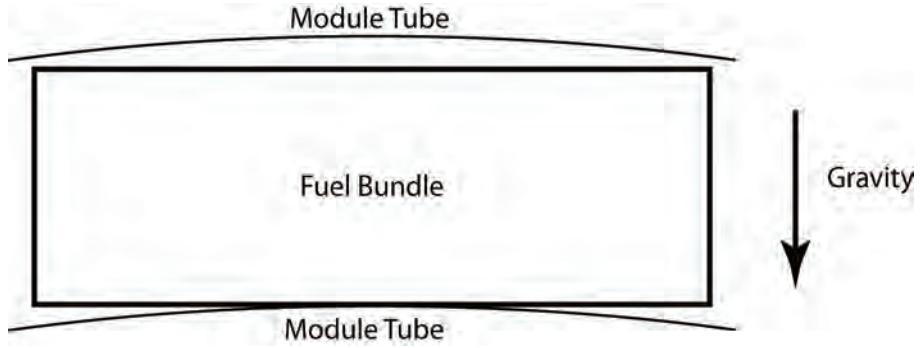
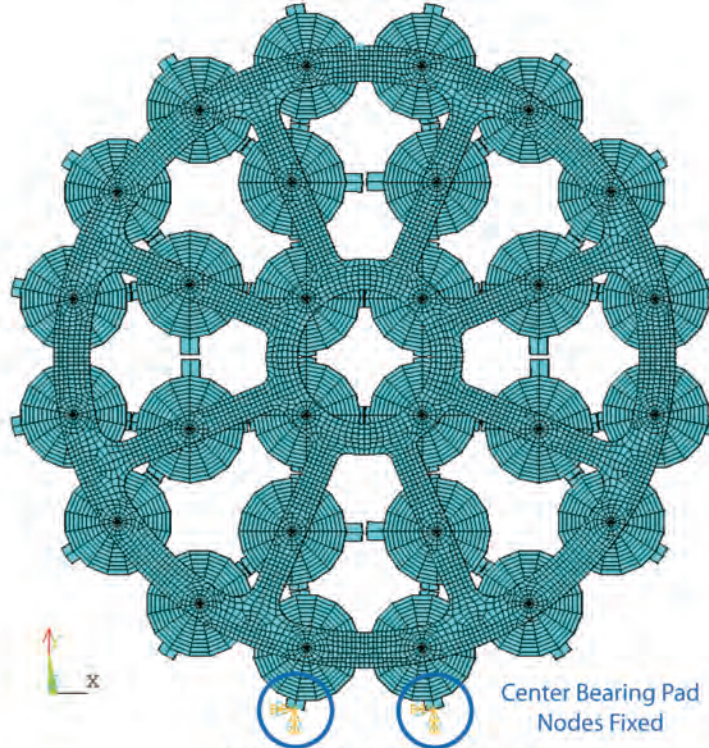


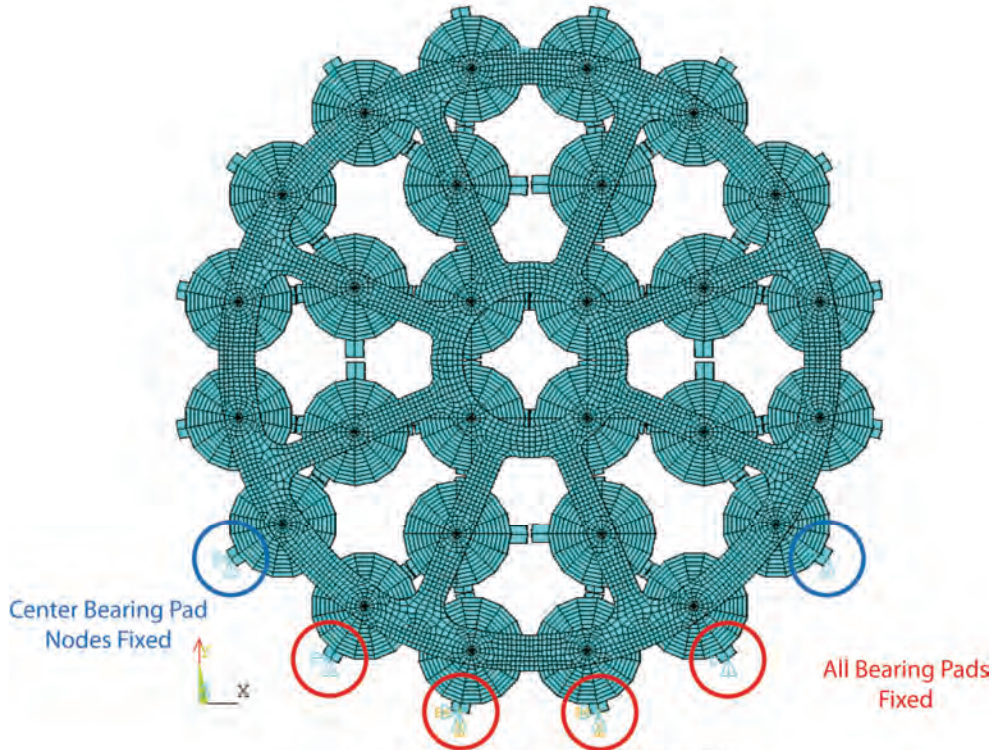
Figure 17: Model Setup for Simulating Crept-Channel Bundle Geometry in a Module Tube

Table 6: Calculated Assembly Weld Maximum Stress Intensity Factors for a Crept-Channel Geometry Bundle in a Module Tube

Element	K_I (MPa m ^{1/2})
11	1.12
12	1.53
22	3.04

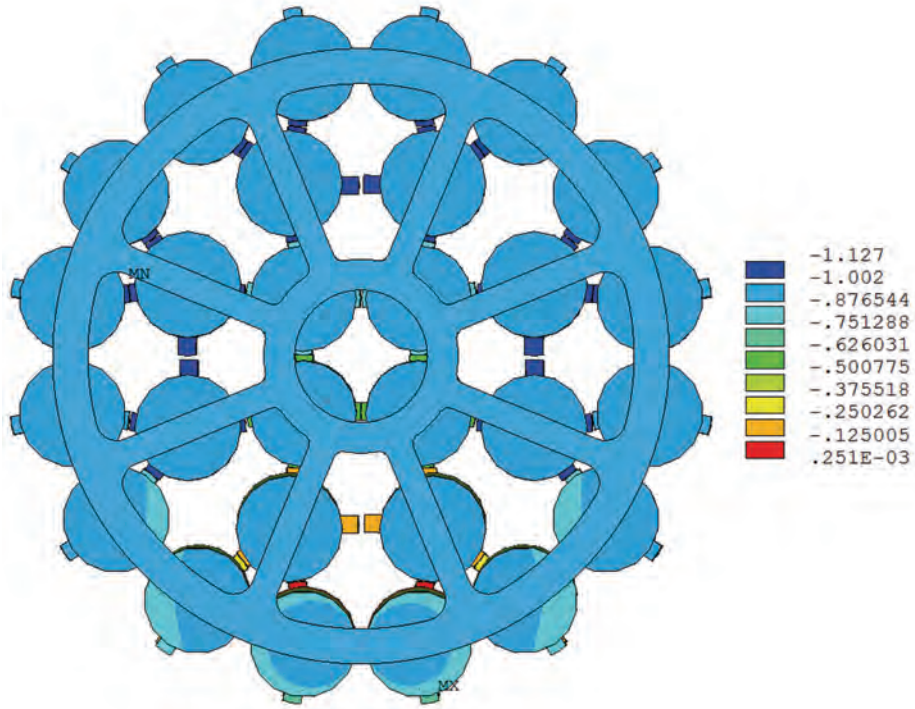


(a) Initial Model Constraints

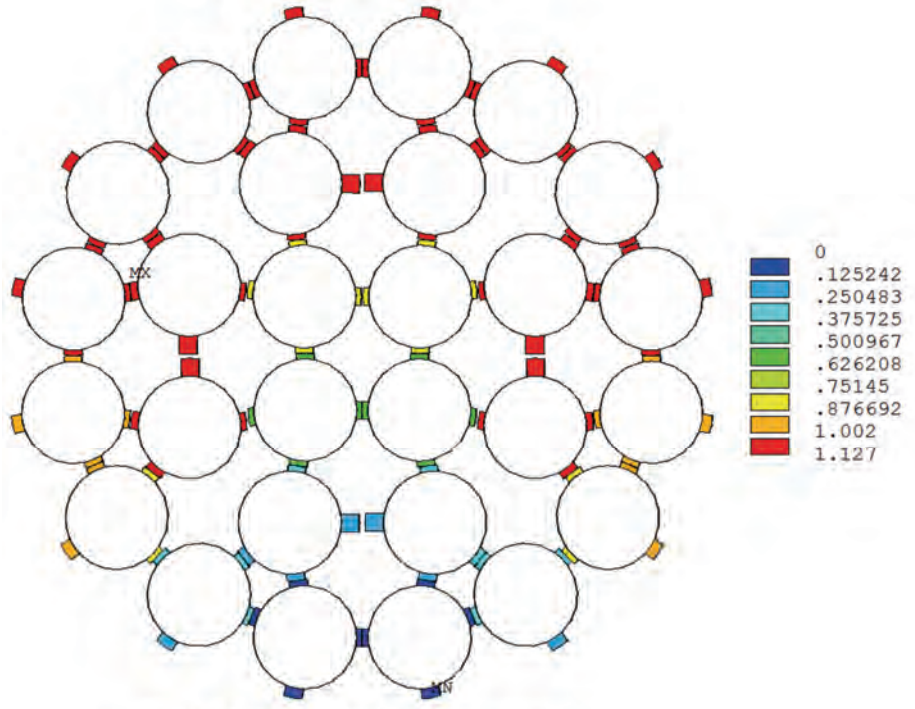


(b) First Iteration Model Constraints

Figure 18: Nodal Constraints Applied to Crept-Channel Bundle Geometry Model



(a) Vertical Displacement (mm)



(b) Mid-Plane Total Displacement (mm)

Figure 19: Displacement of the Fuel Bundle Viewed Along Bundle Axis

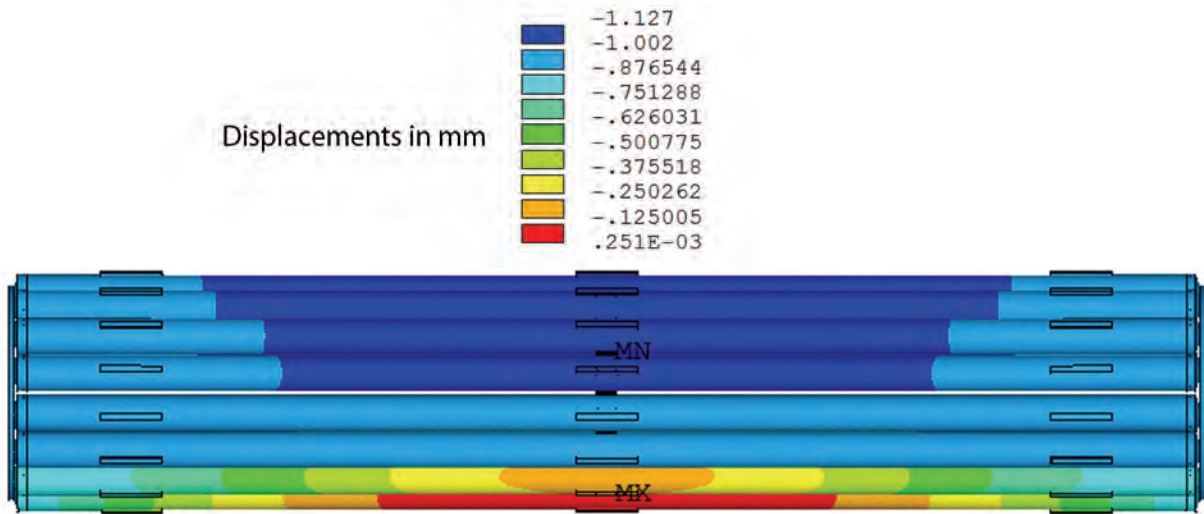
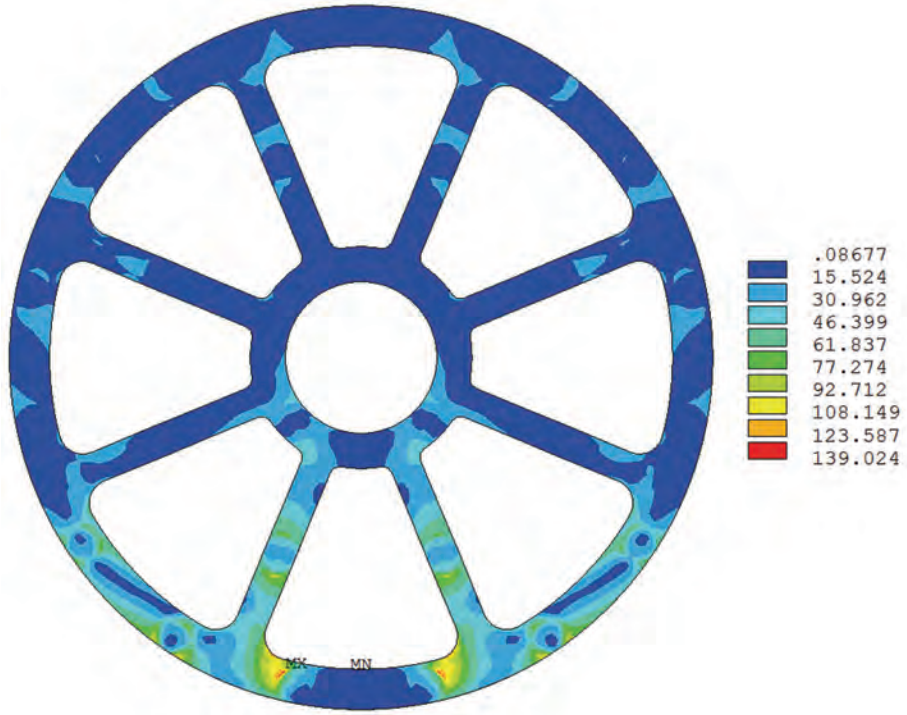
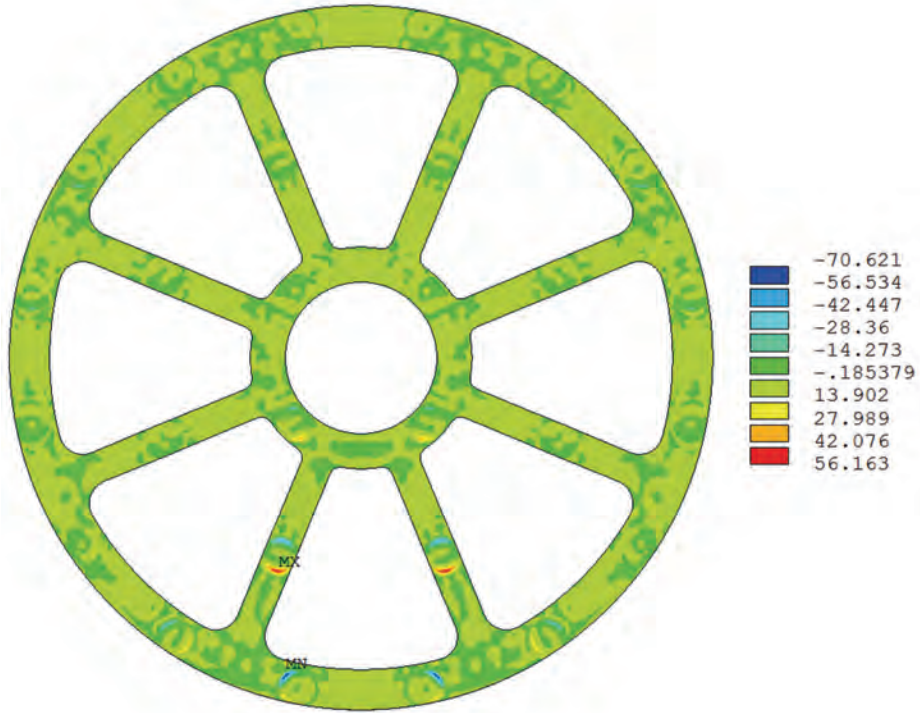


Figure 20: Displacement of the Fuel Bundle Elements From Side View (units in mm)



(a) von Mises (MPa)



(b) Axial Component (MPa)

Figure 21: Endplate Stress Distribution for Crept-Channel Bundle Geometry

3.3 Atypical Fuel Bundle Geometries

In the 2005 Study on the condition of spent CANDU fuel bundles (Lazaroski *et al.*, 2005), visual fuel inspection records of discharged fuel bundles were evaluated to estimate the percentage of fuel in the bulk population that may have increased stress levels in the assembly welds. During fuel inspections, the external surface of the bundle is inspected visually and observations are recorded in accordance with visual standards of deformation, wear, deposits or corrosion, and bundle structural integrity. Records of the observations are made on fuel inspection sheets and evaluated in terms of the effect on the stress levels at the assembly weld. This was then used to estimate the percentage of fuel potentially more susceptible to dry-storage degradation.

The fuel inspection observations that were evaluated that potentially increase the stress levels at the assembly welds in spent fuel bundles are:

- **Crushed bundles**, where there is evidence, or established records, that unusually high loads were applied to the bundles during fuel handling.
- **Dropped bundles**, where there it is known that the fuel bundles were dropped during handling, usually during the process of moving the bundles to the fuel inspection platform.
- **Deformation**, where an observation of abnormal deformation of the bundle was observed. Observations of heavy deformation of the endplate or interlocked spacer pads could potentially increase stress levels, specifically at the assembly welds.
- **Endcap mechanical damage**, where deformation of the endcaps is evident. The interaction causing the damage may affect the residual stress in the assembly weld.
- **Endcap latch marks**, a subset of the previous category where the interaction is due to the fuel channel latches.
- **Missing appendage**, where an element appendage (bearing pad or spacer pad) was not present potentially allowing for greater bowing of the element.
- **Element bowing**, where the abnormal bowing of the element, and possible constraint during dry storage, may increase the stress in the assembly welds.
- **Spacer pad wear**, where significant wear on a spacer pad was observed and would indicate higher-than-normal vibration during irradiation.

For 28-element fuel bundles, no observations of crushed bundles, interlocking spacer pads, endcap latch marks, missing appendages, bowing, or spacer pad wear have been made up to the end of 2004. Several 28-element bundles have been dropped, but these bundles became part of the segregated population and will be stored different than the bulk population. The main non-typical 28-element fuel conditions potentially affecting assembly weld stresses is due to endplate deformation and endcap mechanical damage.

Preliminary calculations assuming small amounts of axial displacement, on the order of tenths of millimetres, applied for a single fuel element can generate significant stresses in the weld crack. To better understand the effect of endplate deformation and endcap mechanical damage have on assembly weld stress levels due to axial deformation, residual stress resulting from the interactions causing such damage would need to be evaluated. This evaluation requires a better understanding of the interactions, the resultant damage, and plastic material properties for irradiated Zr-4. The fuel bundle models would be capable of estimating the stress resulting from such interactions, but further development would be required.

4. SUMMARY AND DISCUSSION OF FINDINGS

The irradiated CANDU fuel bundle model has been used to perform a preliminary evaluation of the stress distributions in endplates and resultant stress intensity factors at the assembly weld cracks of fuel bundles in postulated dry storage conditions. A conservative approach to evaluating the mechanical deformation of spent CANDU fuel bundles in module tubes was employed due to uncertainties in modelling irradiated fuel bundles.

The irradiated 28-element fuel bundle model has been used to calculate the stress distributions and K_I values for several dry storage scenarios. For all these calculations, the hollow fuel element model that ignores stiffening effects of fuel pellets has been used to give conservative results. An evaluation of the endplate stress for fuel bundles with a post-discharge geometry determined from PIE was performed. The maximum stress intensity factor at the tip of a 0.5 mm weld crack in the high-burnup bundle was $0.8 \text{ MPa m}^{1/2}$. The average-burnup bundle calculations gave a higher maximum crack-tip K_I value of $1.5 \text{ MPa m}^{1/2}$. Under gravity and being supported in a module tube, the maximum value of K_I for the average-burnup bundle geometry was approximately $3 \text{ MPa m}^{1/2}$.

There are several sources of uncertainty in these results. First, the fuel bundle geometry has been idealized to the nominal dimensions defined in the fuel design documents and drawings. There are tolerances on the values that the manufacturer must adhere to, but manufacturing dimensions will generally differ from the design values. Wear of the Zr-4 material during irradiation can also affect these dimensions. For example, one important dimension is the spacer pad height. Manufacturing dimensions may be different than modelled, but it is not known if the height is increased or decreased. However, spacer pads do wear during irradiation which will act to increase the gap between mating pads. The amount of wear is highly variable between different bundles as well as within a single bundle and no quantitative data is available on amounts of wear. Therefore, the true gaps between spacer pads are hard to quantify. The radial distance of the element welds from the bundle axis are also variable and can affect the interaction of adjacent elements. Initial endplate deformation may also affect element bending and endplate stress fields. Sensitivity studies using design tolerances could be performed to better understand the effect of bundle dimensions on the endplate stress levels.

Another source of uncertainty in the post-discharge geometry results is the effect of residual stress at the crack tip due to the welding process. Preliminary modelling of the welding process suggests the magnitude of the stress in the weld crack region may be in the vicinity of several hundred MPa. However, stress relaxation due to creep during the bundles' residence in the reactor is expected to be significant and, therefore, the residual stress has been assumed to be negligible in this analysis.

To understand the magnitude of endplate stress resulting from irradiated fuel bundles stored in a DSC, the interaction of a bundle with the module tube was evaluated. This was considered for three bundle geometries: a nominal, straight bundle; a bowed bundle resulting from the sag of the fuel channel in an aged reactor; and a bundle with an average-burnup, post-discharge geometry. The nominal bundle suggests stress intensity factors in the outer-ring elements as large as $1.0 \text{ MPa m}^{1/2}$. The limiting bundle geometry generated a higher maximum stress intensity factor for an outer-ring element of $1.5 \text{ MPa m}^{1/2}$, but the maximum K_I value of $3 \text{ MPa m}^{1/2}$ was calculated for an intermediate-ring element. For the bundle with the post-irradiation

geometry, the highest stress intensity factor was $2.5 \text{ MPa m}^{1/2}$ for an outer-ring fuel element. Further calculations on bundles with post-discharge geometries in module tubes are required to account for sources of uncertainty in these results, which are the post-discharge geometry and the bundle orientation in the module tube.

Outer-ring elements are a primary concern because a loose outer-ring element may interfere with fuel handling systems. Cracking of other elements will likely not result in fuel handling concerns. The analysis performed in this report suggests that the stresses generated in the endplates of irradiated 28-element fuel bundles and resultant stress intensity factors are relatively low. The inner regions of the endplate corresponding to the non-outer-ring elements may have lower stress magnitudes, but bending of these elements may possibly lead to greater stress intensity factors. However, further evaluation of more bundles with a post-discharge geometry simulated in module tubes is required.

5. ACKNOWLEDGEMENTS

The authors would like to thank the various people involved in the work leading to the generation of this publication. Jay Snell at Stern Laboratories performed a series of mechanical deformation tests on unirradiated 28- and 37-element fuel bundles and elements to provide validation of the finite element models. The work of Bogdan Wasiluk and Gordon Shek at Kinectrics was very insightful on the geometries of the assembly welds. Erl Køhn and Steve Wadsworth at AMEC NSS performed a technical review of this document and provided useful feedback and suggestions. Jose Freire-Canosa at the NWMO also contributed greatly to the report with many discussions and suggestions regarding this work.

REFERENCES

- Birch, K., M. Ben Belfadhel, J. Freire-Canosa, F. Garisto, P. Gierszewski, M. Hobbs, T. Kempe, G. Kwong, T. Lam, P. Lum, P. Maak, S. Russell, and A. Vorauer. 2008. Technical research and development program for long-term management of Canada's used nuclear fuel – annual report 2007. Nuclear Waste Management Organization Technical Report TR-2008-01. Toronto, Ontario.
- Lampman, T.J., T.A. Daniels, S. Wadsworth and E. Køhn. 2005. Proposed tests and examinations to provide assurance of fuel integrity during dry storage and subsequent handling. Ontario Power Generation, Nuclear Waste Management Division Report 06819-REP-03720-00009-R00. Toronto, Ontario.
- Lampman, T.J., A. Popescu, and J. Freire-Canosa. 2009. Comparison of CANDU fuel bundle finite element model with unirradiated mechanical load experiments. Journal of ASTM International, Volume 6, Number 3. West Conshohocken, USA.
- Lazaroski, M., T. Lampman, S. Wadsworth, and E. Køhn. 2005. Reference fuel characteristics at the start of dry storage. Ontario Power Generation, Nuclear Waste Management Division Report 06819-REP-03720-00007-R00. Toronto, Ontario.
- Lovasic, Z. and J.E. Villagran. 2004. Used fuel integrity during dry storage: investigation program. Ontario Power Generation, Nuclear Waste Management Division Technical Memo 06819-REP-03720-00006-R00. Toronto, Ontario.
- MATPRO. 1990. SCDAP/RELAP5/MOD2 code manual, volume 4: MATPRO – a library of materials properties for light-water-reactor accident analysis. NUREG/CR-5273, EGG-2555, Volume 4 R3.
- MATPRO. 2003. SCADAP/RELAP5-3D code manual volume 4: MATPRO – a library of materials properties for light-water-reactor accident analysis. INEEL/EXT-02-00589, Volume 4, Revision 2.2.
- Popescu, A. and T. Lampman. 2010. CANDU fuel element model development and sensitivity study. Nuclear Waste Management Technical Report TR-2010-12. Toronto, Ontario.
- Shek, G.K. and B.S. Wasiluk. 2010. Development of Delayed Hydride Cracking Test Apparatus and Commissioning Tests for CANDU Fuel Bundle Assembly Welds. Nuclear Waste Management Organization Technical Report TR-2009-08, Toronto, Ontario.
- Snell, J. 2007. Mechanical deformation tests on 37 and 28 element fuel. Stern Laboratories Report SL-190. Hamilton, Ontario.
- Snell, J. 2009. Mechanical deformation tests on 37 and 28 element fuel elements. Stern Laboratories Report SL-205. Hamilton, Ontario.